



ELSEVIER

Contents lists available at ScienceDirect



New paleoenvironmental proxies for the Irati black shales (Paraná Basin, Brazil) based on acidic NSO compounds revealed by ultra-high resolution mass spectrometry

Laercio L. Martins ^{a,b,*}, Hans-Martin Schulz ^a, Mareike Noah ^a, Stefanie Poetz ^a, Hélio Jorge P. Severiano Ribeiro ^b, Georgiana F. da Cruz ^b

^a GFZ German Research Centre for Geosciences, Sec. 3.2 Organic Geochemistry, Telegrafenberg D-14473, Germany

^b Laboratory of Petroleum Engineering and Exploration (LENEP), North Fluminense State University (UENF), Macaé, Rio de Janeiro 27910-970, Brazil



ARTICLE INFO

Article history:

Received 8 August 2020

Received in revised form 30 October 2020

Accepted 6 November 2020

Available online 10 November 2020

Keywords:

Paraná Basin

Irati Formation

Black shale

Paleosalinity

Heteroatom compounds

Acidic biomarkers

Isoprenoidyl phenols

Petroleomics

ESI(-) FT-ICR-MS

ABSTRACT

Variations of the acidic NSO (Nitrogen, Sulphur, and Oxygen) compound composition of the Lower Permian Irati black shales and Serra Alta shales were assessed by Fourier transform ion cyclotron resonance mass spectrometry (FT-ICR-MS) using electrospray ionization (ESI) in negative ion mode to test their significance for the regional paleoenvironmental reconstruction by comparison with known features in the northeastern and central-eastern Paraná Basin, Brazil. The high abundance of the S_1O_X class for the basal Irati black shales in the northeastern basin reflects a sulfide-rich environment, whereas high $O_{>2}$ classes in the Serra Alta shales indicate a high input of terrestrial organic matter deposited in oxic waters. Here, eight parameters based on O_1 and O_2 compounds are suggested as new paleoenvironmental proxies: phenol index (%DBE 4; O_1 class); C_{27}/C_{28} DBE 4 (O_1 class); C_{27}/C_{28} DBE 5 (O_1 class); Even/Odd_{FA}; TAR_{FA} Odd (terrigenous/aquatic ratio); TAR_{FA} Even; C_{36} hopanoic acid index; and hopanoic/steranoic acids ratio. Higher values of the phenol index, the TAR_{FA} and Even/Odd_{FA} indicate higher land plant input during the final black shale deposition. Variations of C_{27}/C_{28} DBE 4 and C_{27}/C_{28} DBE 5, the first being based on the distribution of methylated isoprenoidyl phenols, can be used to reconstruct paleosalinity; here higher values indicate higher salinity. The C_{36} hopanoic acid index is higher for the marine hypersaline samples from the northeastern basin, while a significant bacterial biomass signal is stored as a higher hopanoic/steranoic acids ratio for samples from the central-eastern basin.

© 2020 Elsevier Ltd. All rights reserved.

1. Introduction

Ultra-high resolution mass spectrometry has been widely used to assess the polar composition of crude oils and organic extracts of source rocks as well as their subfractions on the molecular level in order to obtain geochemical information and to infer oil properties (Hughey et al., 2002; Rodgers et al., 2005; Niyonsaba et al., 2019; Borisov et al., 2019), mostly in direct infusion experiments (Marshall and Rodgers, 2004). The technique offers a broad range of different applications, especially in petroleum geology, e.g., to assess the degree of oil biodegradation (Kim et al., 2005; Vaz et al., 2013b; Martins et al., 2017) or to evaluate oil acidity (Vaz et al., 2013a; Terra et al., 2014), to unravel petroleum migration

and fractionation (Han et al., 2018a, b; Ziegs et al., 2018a) or source rock and oil maturity (Hughey et al., 2004; Oldenburg et al., 2014; Poetz et al., 2014; Hosseini et al., 2017), and to reconstruct depositional paleoenvironments (Wan et al., 2017; Ji et al., 2018; Rocha et al., 2019).

Fourier transform ion cyclotron resonance mass spectrometry (FT-ICR-MS) is capable of providing the necessary ultra-high mass resolution and accuracy for a molecular assessment (Vanini et al., 2020), attributing formulas to thousands of polar components with medium to high molecular weights ($m/z > 150$ Da) in highly complex natural or industrial mixtures (e.g., >49,000 compounds detected in a heavy petroleum distillate by 21 T FT-ICR-MS according to Smith et al., 2018). Such analytical potential is a step forward in comparison to traditional gas chromatography-mass spectrometry approaches (Marshall and Rodgers, 2004; Rodgers et al., 2005; Marshall et al., 2007; Rodgers and McKenna, 2011; Han et al., 2018a). Employing ionization techniques such as electrospray ionization (ESI), FT-ICR-MS unambiguously identifies ele-

* Corresponding author at: Laboratory of Petroleum Engineering and Exploration (LENEP), North Fluminense State University (UENF), Amaral Peixoto Road, Km 163, Brennand Avenue, Imboassica, Macaé, Rio de Janeiro 27925-535, Brazil.

E-mail address: laercio@lenep.uenf.br (L.L. Martins).

mentary compositions which can be further broken down according to the heteroatom classes (NnOoSs), double bond equivalents (DBEs) that are related to the number of rings plus double bonds involving carbon, and carbon numbers (CNs; Marshall and Rodgers, 2008). Using the negative ion mode, the ESI technique enables optimum detection of acidic NSO compounds that are capable to deprotonate, such as carboxylic acids, phenols, alcohols (e.g., aromatic alcohols), or pyrroles (Qian et al., 2001; Kim et al., 2005; Oldenburg et al., 2014).

Acidic NSO compounds in sediments store a wealth of geological information, but were never calibrated against known hydrocarbon biomarkers and their meaning (e.g., marine vs. terrestrial organic matter (OM), photic zone euxinia, etc.). For this, an OM-bearing sedimentary succession is needed of preferentially low thermal maturity and well-resolved and known paleoceanographic signals. We have chosen the Irati Formation, which was deposited at 278.4 ± 2.2 Ma in the Artinskian/Kungurian age of the Permian period (Fig. 1a; Santos et al., 2006; Rocha-Campos et al., 2011). It documents a unique moment in the evolution of the Paraná Basin (Brazil) at the southern margin of breaking through Gondwana when the water circulation between the basin and the Panthalassa ocean was restricted leading to a hypersaline environment in the interior basin (Milani et al., 2007a). Hence, organic-rich shales accumulated in the southern, central-eastern, and northeastern Paraná Basin (Zalán et al., 1990). These shales have total organic carbon (TOC) contents that reach one of the highest levels ever recorded in sedimentary systems (up to 26 wt% TOC; Faure and Cole, 1999; Milani et al., 2007a) with a high potential for oil generation (Araújo et al., 2000).

Irati black shales and related oils are known for their content of acidic polar compounds, including phenols, carboxylic acids, and sulfur compounds such as alkylthiophenes (Carvalhaes and Cardoso, 1986; Afonso et al., 1992a, b). Moreover, the Irati oil shales obtained by the Petrosix Process have on average 0.82 wt% of sulfur and 0.93 wt% nitrogen contents (Afonso et al., 1992b). Against this background, we applied a two-stage conceptual approach. First, we identified and determined the acidic NSO composition of the Irati black shales and the overlying Serra Alta shales in detail by means of ESI(-) FT-ICR-MS. Second, we compared these data with established hydrocarbon proxies and their meaning about the depositional system (Martins et al., 2020a, b). It is thus the ultimate goal of this study to highlight the geochemical relevance of acidic polar compounds and to establish their significance as keys to investigate the depositional environment of sediments and their controlling factors.

2. Experimental

2.1. Samples

The sample set comprises 17 outcrop samples of the Irati Formation (previously investigated by Martins et al., 2020a, b) and three outcrop samples from the Serra Alta Formation, which were collected at two sites in the Paraná Basin (Fig. 1b). Ten Irati samples are black shales from a quarry in São Mateus do Sul City (State of Paraná; central-eastern basin). Here, the immature black shale sustains an industrial plant that converts the organic matter (OM) via the Petrosix process to oil and gas (Milani et al., 2007b). Further seven Irati samples are black shales collected from a quarry in the area of Amaral Machado Mining Company (Satinho city, State of São Paulo; northeastern basin), and shale samples from the Serra Alta Formation were also collected in this quarry.

Samples from the quarry in São Mateus do Sul were collected from two different stratigraphic horizons of the Irati Formation. The lower and upper units (according to Correa da Silva and Cornford, 1985) correspond to the chemostratigraphic units E

and H, respectively (according to Reis et al., 2018; Fig. 1a). The samples from the quarry in the Amaral Machado area belong to the chemostratigraphic unit H (according to Reis et al., 2018). Samples were collected from the base to the top in these chemostratigraphic units.

2.2. TOC and Rock-Eval

TOC determination and Rock-Eval pyrolysis were performed by Applied Petroleum Technology (APT) AS (Oslo, Norway), according to the methodology presented in Martins et al. (2020a). Jet-Rock was run on every tenth sample as an external standard and checked against the acceptable range given in NIGOGA (4th Edition; Weiss et al., 2000).

2.3. Extraction

Approximately 90–150 g of the rock samples were crushed and pulverized prior to extraction with 300 mL dichloromethane (chromatographic grade from Sigma-Aldrich) using a Soxhlet system for 48 h. The obtained organic extracts were gravimetrically determined after the removal of the solvent. Elemental sulfur was removed from organic extracts (25 mg on average) of the Serra Alta shales passing it through a colloidal copper column (Blumer, 1957), using 20 mL of dichloromethane and 20 mL of methanol.

2.4. GC-FID and GC-MS

Asphaltenes were precipitated from the organic extracts using an excess of *n*-hexane (after adding a small volume of dichloromethane:methanol, 99:1) in an ultrasonic bath for 10 min, followed by filtration via Na₂SO₄ in a glass funnel and by intensive washing with *n*-hexane and the remaining maltenes were separated into saturate, aromatic, and NSO fractions by Medium Pressure Liquid Chromatography (MPLC, according to Radke et al., 1980). The aliphatic fractions were analyzed by gas chromatography with flame ionization detection (GC-FID) using an Agilent 6890 device equipped with an HP Ultra 1 capillary column (50 m × 0.2 mm × 0.33 μm), according to Martins et al. (2020a). 5α-Androstane (5 mg mL⁻¹) was used as an internal standard for the quantification of *n*-alkanes, pristane (Pr), and phytane (Ph). The aliphatic, aromatic, and NSO fractions were analyzed by a DSQ Thermo Finnigan Quadrupole MS coupled to a gas chromatograph (GC-MS, according to Martins et al., 2020a). The GC was equipped with a Thermo PTV injection system (Thermo Electron Corporation) and a BPX5 (SGE) capillary column (50 m × 0.22 mm × 0.25 μm). Full scan mass spectra were recorded from 50 to 600 Da at a scan rate of 1.5 scans s⁻¹. The hopanes and steranes were monitored using *m/z* 191 and 217, respectively. The 8-methyl-MTTC (Me-MTTC, MTTC as methyltrimethyltridecylchroman) was monitored using *m/z* 121, and the 5,8- and 7,8-dimethyl-MTTCS (diMe-MTTCS) were monitored using *m/z* 135. The NSO fractions of ten selected samples of the Irati Formation (AMa 1, 7, 11, 23, and 24; SM 2.1, 2.2, 2.4, 3.5, and 3.7; based on ESI(-) FT-ICR-MS results) were silylated prior to GC-MS analysis using N-methyl-N-(trimethylsilyl)-trifluoroacetamide (MSTFA), and the trimethylsilyl ethers of the methyl-, dimethyl- and trimethyl-isoprenoidyl phenols were monitored using *m/z* 194, 208, and 222, respectively.

2.5. ESI(-) FT-ICR-MS

For each extract of the Irati and Serra Alta samples, a stock solution was prepared with a concentration of 1 mg mL⁻¹ in methanol and toluene (v/v = 1:1), which was diluted to reach a final concentration of 100 μg mL⁻¹ using the same solvent mixture. To promote

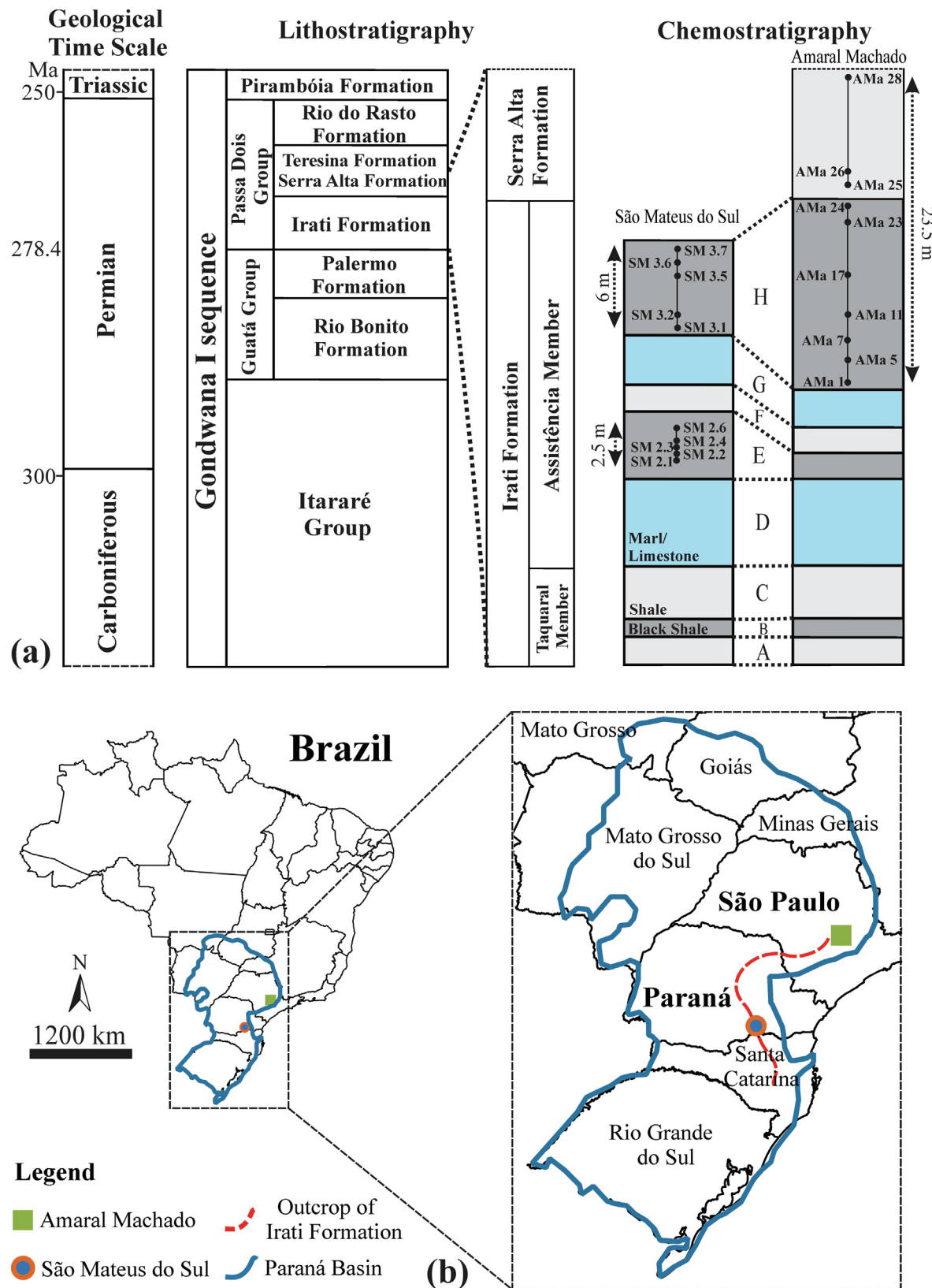


Fig. 1. Geological time scale (modified after Santos et al., 2006, and Milani et al., 2007b) with integrated lithostratigraphy of the “Gondwana I” sequence of the Paraná Basin (Milani et al., 2007b), and the correlation between the Irati black shales used in this work and their chemostratigraphic units E and H (Reis et al., 2018; Martins et al., 2020a) that correspond to the lower and upper units, respectively (Correia da Silva and Cornford, 1985). The geographic location of the Paraná Basin and the localities of the two sampling areas (b): Amaral Machado Quarry in the State of São Paulo (northeastern basin); São Mateus do Sul Quarry in the State of Paraná (central-eastern basin). Dashed red line shows the occurrence of the Irati outcrops along the basin margin. (For interpretation of the references to colour in this figure legend, the reader is referred to the web version of this article.)

the deprotonation of the sample constituents, a concentrated aqueous NH₃ solution (10 µL) was added to 1 mL sample solution.

Mass analyses were performed in negative ion ESI mode with a 12 T FT-ICR mass spectrometer equipped with an Apollo II ESI source from Bruker Daltonik GmbH (Bremen, Germany) according to Poetz et al. (2014). Nitrogen was used as drying gas at a flow rate of 4.0 L min⁻¹ and a temperature of 220 °C and as nebulizing gas with 1.4 bar. The sample solutions were infused at a flow rate of 150 µL h⁻¹. The capillary voltage was set to 3,000 V and an additional collision-induced dissociation voltage of 70 V in the source was applied to avoid cluster and adduct formation. Ions were accumulated in the collision cell for 0.05 s and transferred to the ICR cell within 1 ms. Spectra were recorded in broadband mode using four mega word data sets. For each mass spectrum, 200 scans have been accumulated in a mass range from *m/z* 147 to 1,000. Sine-bell apodization was applied before the Fourier transformation to produce the frequency domain data, which were then converted to the mass spectrum.

After external calibration, all spectra were internally recalibrated in a quadratic calibration mode using the most prominent homologue series of O₁, O₂ or N₁ compounds within each spectrum. Elemental formulas were assigned to all peaks with signal to noise ratios above 12 with a maximum error of 0.5 ppm allowing 0–100C, 0–200H; 0–8O, 0–2N, 0–2S, 0–1Na, and 0–2 ¹³C isotopes. Elemental formulas were sorted according to their heteroatom class (N_yO_xS_z; elemental class), compound class, DBE, and CN. The abundances of grouped (elemental, compound, and DBE classes) as well as of individual peaks are given as Total Monoisotopic Ion Abundances (% TMIA) in this work, which refers to the abundance of grouped or individual monoisotopic peaks in relation to the abundance of all monoisotopic peaks. More details regarding the mass calibration and the analytical approach are described in Poetz et al. (2014).

3. Results

3.1. Elemental class distribution

The elemental class distributions of the Irati black shale extracts from the Amaral Machado Quarry (sample details in Fig. 1a) are pre-

sented in Table 1 showing the four most abundant classes (see also the pie charts in the Supplementary material Fig. S1). Table 1 also presents the monoisotopic assigned ions usually over 80% of all detected peaks, the mean molecular weight normalized to the number of signals (Mn), and the molecular weight (Mw). The O_x class dominates the samples, possibly due to their low maturity (Poetz et al., 2014), ranging from 41.1 to 57.3% TMIA. The N_yO_x class is in general the second largest one, ranging from 12.4 to 33.0% TMIA, followed by the N_y class ranging from 11.2 to 25.1% TMIA. The S_zO_x class comprises 0.0 to 27.2% TMIA and shows a striking decrease toward the top of the unit (AMa 1 to AMa 24). The O_xNa₁ class is present in the samples, ranging from 1.0 to 5.0% TMIA. N_yS_z and N_yO_xS_z classes also occur in the samples, but lower than 0.5% TMIA. The Amaral Machado profile about the elemental class distribution is completed by three shale extracts from the Serra Alta Formation (AMa 25, 26, and 28; Table 1; Fig. S1a). The oxygen containing classes markedly dominate the spectra of these samples, with a high abundance of the O_x class (75.4–80.2% TMIA), followed by the S_zO_x class (7.3–13.5% TMIA), O_xNa₁ class (6.5–8.2% TMIA), and N_yO_x class (1.5–7.2% TMIA). The N_yS_z and N_yO_xS_z classes are only present in low abundance (lower than 1.0% TMIA), and the N_y class is almost absent (maximum of 0.1% TMIA).

The elemental class distribution of the Irati black shale extracts from the lower and the upper unit in the São Mateus do Sul area are presented in Table 1 showing the four most abundant classes (see the pie charts in Fig. S1b). In accordance to the Amaral Machado samples, the O_x class dominates the samples ranging from 38.6 to 63.2% TMIA (except for sample SM 3.7). The N_y class is second most abundant for samples from the lower unit (10.1–33.9% TMIA) and third most for samples from the upper unit (15.9–19.9% TMIA), while the trend is opposite for the N_yO_x class. The O_xNa₁ class mainly represents multimers of O_x compounds that are formed during the ionization process and range from 2.6 to 14.1% TMIA. The S_zO_x class with 0.1–3.7% TMIA is only a minor constituent and shows higher values for samples from the lower unit. N_yS_z is also present in the samples, but with low abundance (<0.3% TMIA).

3.2. Compound class distribution

Fig. 2 shows the compound class distribution of the four most abundant elemental classes in the Irati black shales and the Serra

Table 1

TOC contents and Rock-Eval data on the left, completed to the right by number of signals, average molecular weights, and percentages of the most abundant NSO classes (from FT-ICR-MS analysis) of the investigated shale samples from the Irati and the Serra Alta Formation.

Location	Formation/ unit	Sample	TOC (wt. %)	Rock Eval			ESI(-) FT-ICR-MS						
				Tmax (°C)	HI (mg HC/g TOC)	OI (mg CO ₂ /g TOC)	No. signal	Mn	Mw	O _x (%) TMIA)	N _y (%) TMIA)	N _y O _x (%) TMIA)	S _z O _x (%) TMIA)
Amaral Machado	Serra Alta	AMa 28	0.28	427	32	323	1545	412	431	76.1	0.1	7.2	7.3
		AMa 26	0.45	426	54	126	1477	420	438	80.2	0.0	1.5	10.4
		AMa 25	0.42	422	48	157	1697	424	442	75.4	0.1	3.8	13.5
		Irati					2008	442	464	57.3	21.1	16.1	0.0
		AMa 24	5.57	438	602	4	2389	453	474	42.5	22.8	33.0	0.0
		AMa 23	4.51	420	433	6	2264	407	425	53.9	11.2	29.3	3.3
		AMa 17	6.47	429	519	7	2161	439	461	45.9	23.4	27.6	0.6
		AMa 11	6.77	423	539	11	2085	431	451	41.1	25.1	25.5	7.3
		AMa 7	6.05	424	543	17	2347	432	455	48.6	17.7	22.7	7.2
São Mateus do Sul	Irati (Upper unit)	AMa 5	4.85	404	348	20	2051	438	457	42.5	16.0	12.4	27.2
		AMa 1	4.14	405	490	29	2257	446	465	38.6	15.9	41.1	0.5
		SM 3.7	22.10	425	421	6	2285	449	470	53.0	19.9	22.0	0.3
		SM 3.6	13.10	423	603	6	2181	461	483	53.1	19.3	20.7	0.1
		SM 3.5	12.50	430	631	6	2075	448	468	53.9	16.6	20.1	0.1
		SM 3.2	10.80	423	595	6	2244	450	472	49.0	19.9	23.5	0.2
	Irati (Lower unit)	SM 3.1	8.88	424	561	5	2147	443	464	63.2	10.1	9.8	2.6
		SM 2.6	4.55	428	471	9	1708	435	454	40.9	30.6	23.8	0.4
		SM 2.4	18.70	427	535	3	2044	459	483	41.2	32.7	19.5	2.6
		SM 2.3	10.80	427	598	2	2016	472	500	44.1	33.9	15.7	3.7
		SM 2.2	8.37	424	583	3	1814	421	441	52.2	27.3	13.3	3.0
		SM 2.1	5.74	420	505	6							

No. signals: number of monoisotopic assigned ions; Mn: number-average molecular weight; Mw: weight-average molecular weight.

Alta shales (O_x , N_y , N_yO_x , and S_zO_x). The most abundant O_x class comprises mainly O_1 , O_2 , O_3 , and O_4 compounds within the Irati black shales, while the Serra Alta shales primarily consist of more oxygenated compounds with two to seven oxygen atoms, likely related to the predominant input of terrigenous OM (Martins et al., 2020c). The second most abundant N_y class comprises mostly N_1 compounds, except for samples AMA 23 and 24 that also contain N_2 compounds. N_y compounds are nearly absent in the Serra Alta Formation. In contrast, samples from the lower unit in the São Mateus do Sul area have a markedly higher relative intensity of the N_1 class than samples from the upper unit, except for their top sample SM 2.6.

The N_yO_x class comprises mainly N_1O_1 and N_1O_2 compounds, followed by N_1O_3 , N_2O_1 , and N_2O_2 (Fig. 2). N_yO_x compounds are few in the Serra Alta shales, while the topmost sample of the upper unit in the São Mateus do Sul area shows a markedly higher amount of N_yO_x compounds, here mostly of the more oxygenated ones. The S_zO_x class in both the Irati black shales and the Serra Alta shales is dominated by S_1O_4 compounds. The notably higher amounts of the S_1O_4 class in the Irati black shales from the Amaral Machado area are likely related to its shallower marine depositional environment with higher salinity and more reducing conditions (Martins et al., 2020a), followed by the Irati black shales from the lower unit of the São Mateus do Sul area where they decrease toward the top of these units.

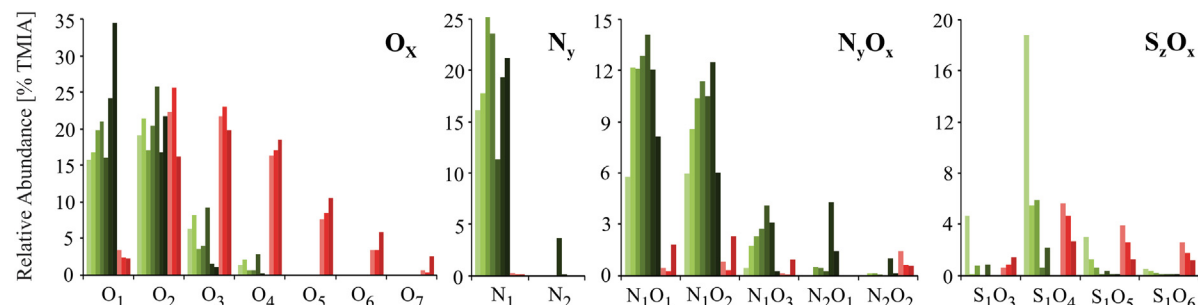
3.3. DBE and CN distributions of NSO classes

The DBE distribution of the N_1 class in the Irati black shales from both localities (Fig. S2a and b) ranges from DBE 6 to 23 (plots of DBE versus CN in the Fig. S3), which is consistent with the DBE range of pyrrolic nitrogen compounds published by e.g., Shi et al.

(2010), Poetz et al. (2014), and Oldenburg et al. (2014). Such compounds are commonly found in rocks deposited in both marine (Clegg et al., 1997) and non-marine environments (Zhang et al., 2008). Here, the N_1 DBE distributions have similar patterns and differ mainly in the relative abundance of individual DBE classes. The N_1 profiles of the Irati black shales resemble those of immature shales as, for example, the Lower Jurassic TOC-rich Posidonia Shale with a thermal maturity between 0.48 and 0.53 % vitrinite reflectance R_o (Poetz et al., 2014). In such shale, a relatively low abundance of compounds with high DBE, such as dibenzocarbazoles (III, DBE 15) and benzonaphthocarbazoles (IV, DBE 18), and a higher abundance of compounds with low DBE, such as carbazoles (I, DBE 9) and benzocarbazoles (II, DBE 12) is observed. N_1 compounds with DBE 6, 7, and 8 are absent in samples AMA 1 and 5 (Fig. S3) probably due to their slightly higher maturity.

The DBE distribution of the O_1 class in the Serra Alta shale (Fig. 3a), and the Irati black shales from Amaral Machado (Fig. 3b) and São Mateus do Sul (Fig. 3c) ranges from DBE 1 to 17. O_1 compounds that are detected by ESI(-) FT-ICR-MS are mainly compounds with a hydroxyl functional group that is sufficiently acidic to be deprotonated, such as phenols (Hughey et al., 2002; Kim et al., 2005). In general, the DBE distribution of the O_1 class shows a maximum for compounds with DBE 4 (V) or DBE 5 (VI; see also in the plots of DBE versus CN in the Fig. S4). The compounds with DBE 4 are likely alkylphenols (Shi et al., 2010; Ji et al., 2018) while those with DBE 5 are considered as indanols and 5,6,7,8-tetrahydronaphthalenols (Ji et al., 2018). These assumptions are supported by results from Afonso et al. (1992b) who showed that alkylphenols are the most abundant acidic oxygen compounds generated from the Irati Shale from São Mateus do Sul in the Petrosix Process (4 wt% using esterification before analysis by GC-MS). The slightly higher abundance of O_1 com-

Amaral Machado



São Mateus do Sul

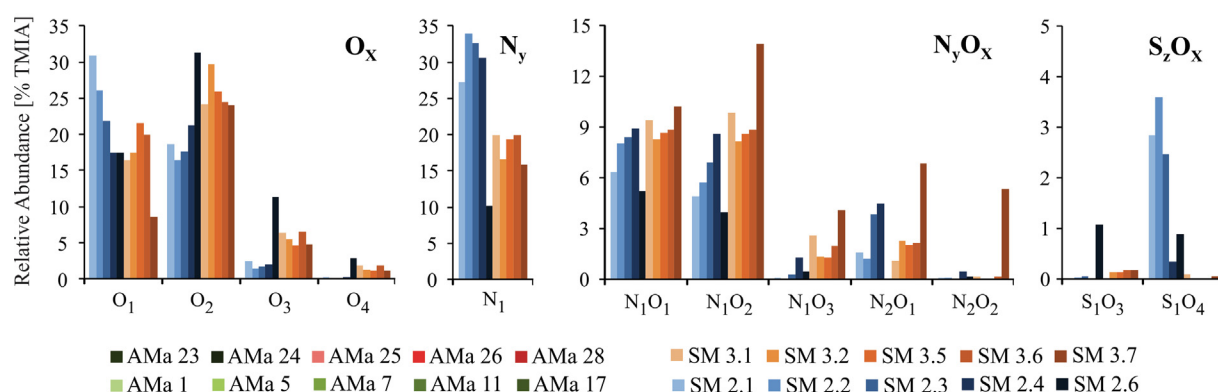


Fig. 2. Compound class distributions of the O_x , N_y , N_yO_x , and S_zO_x classes in the extracts of the 17 Irati black shales and three Serra Alta shales from Amaral Machado and São Mateus do Sul areas.

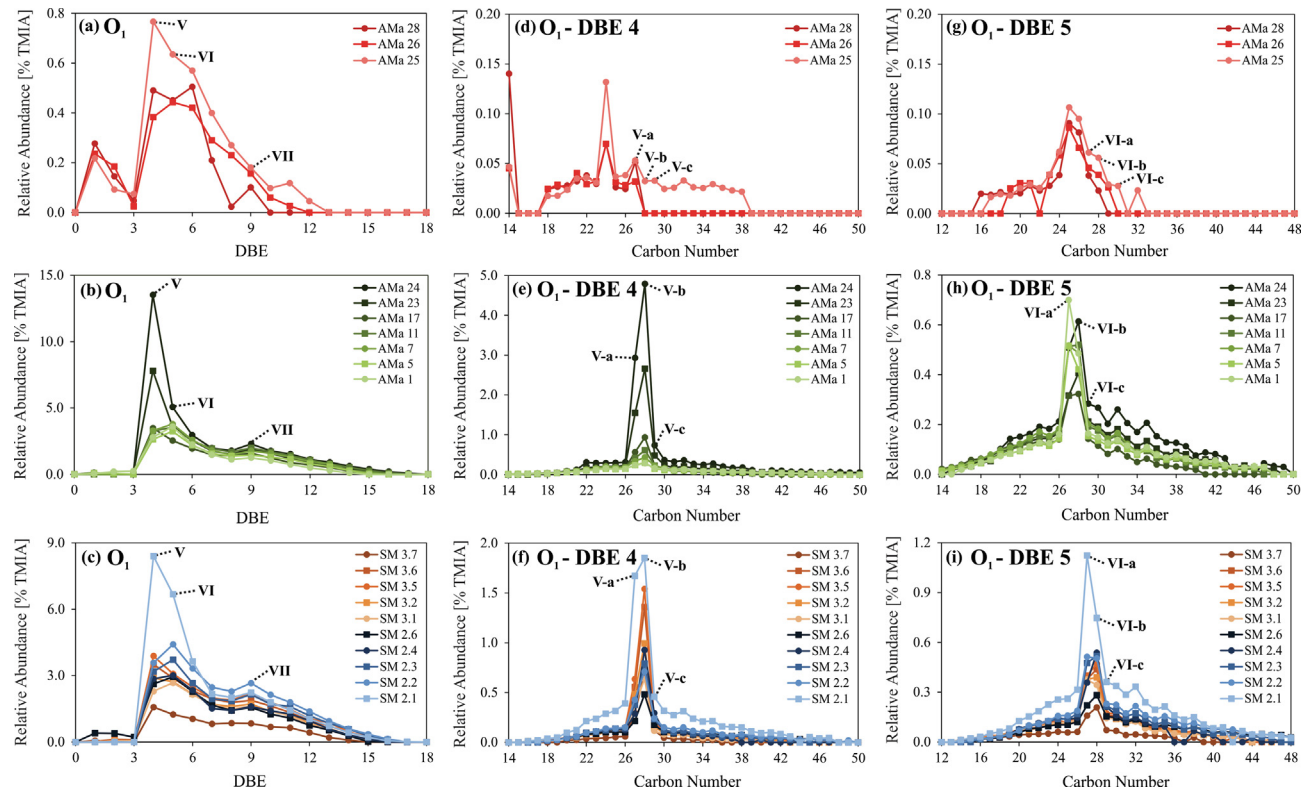


Fig. 3. DBE distribution of the O_1 class in the Serra Alta shales (a), and Irati black shales from Amaral Machado (b) and São Mateus do Sul (c) areas. CN distributions for O_1 -DBE 4 and 5 classes in the Serra Alta shales (d and g), and Irati black shales from Amaral Machado (e and h) and São Mateus do Sul (f and i) areas.

pounds with DBE 9 (**VII**) could possibly be attributed to fluorenols. The relative abundance of the O_1 compounds decreases with increasing DBE.

The CN distribution of the most abundant O_1 compounds with DBE 4 typically ranges from CN 14 to 50 (Fig. 3d, e, and f). Remarkable are the higher abundances of the DBE 4 O_1 compounds with CN 27 (**V-a**; C_{27}), 28 (**V-b**; C_{28}), and 29 (**V-c**; C_{29} ; Fig. S4). These compounds occur to a minor degree in crude oils (analysis by ESI (-) FT-ICR-MS) and were interpreted as sterol-like compounds (Shi et al., 2010; Oldenburg et al., 2014; Rocha et al., 2018, 2019). However, sterols lose their hydroxyl functional group during diagenesis and are rarely reported in crude oil analyses (Oldenburg et al., 2014). Here, we clearly demonstrate that these elemental compositions represent mainly methyl-, dimethyl-, and trimethyl-isoprenoidyl phenols (C_{27} - C_{29} , **V**; plausible structures of **V** to **X** compounds in Appendix A), using GC-MS analysis of the silylated NSO fraction of the Irati black shale extracts. The trimethylsilyl ether derivatives of these compounds (**V-a'**, **V-b'**, and **V-c'**; Simoneit et al., 1996; Zhang et al., 2011) are detected in high amounts in the ion traces m/z 194 + 208 + 222 of the mass chromatograms shown in Fig. 4 (see the mass spectra for compounds **V-a'**, **V-b'**, and **V-c'** in the Fig. S5). The relative distribution of the derivatized methylated isoprenoidyl phenols (Fig. 4) correlates well with the FT-ICR-MS derived distribution of the CN 27 to 29 DBE 4 O_1 compounds (see the positive correlation between the C_{27} / C_{28} DBE 4 O_1 compounds ratio and the C_{27} / C_{28} isoprenoidyl phenols-TMS ratio in Fig. S6; see their values for representative samples in Fig. 4). Dimethyl-isoprenoidyl phenols (**V-b**) predominate over the others isoprenoidyl phenols in all samples, except for sample SM 2.1 that is characterized by a slightly higher abundance of the methylated one (**V-a**; C_{27} / C_{28} isoprenoidyl phenols-TMS > 1 in Fig. 4). Both methyl- and dimethyl-isoprenoidyl phenols occur in high amounts and dominate in samples AMA 23 and 24

(Fig. 4), in accordance with the higher abundance to the CN 27 and 28 DBE 4 O_1 compounds in these samples (Fig. 3).

The isoprenoidyl phenols are known from various petroleum fluids (Simoneit et al., 1996; Barak and Rullkötter, 1997; Zhang et al., 2011, 2019; Barakat et al., 2012; Liu et al., 2015), and the proposed structures indicate that their precursors are structurally related to chromans (Simoneit et al., 1996), which were already found in the here investigated Irati black shales (Martins et al., 2019, 2020a). The low occurrence of isoprenoidyl phenols in crude oils is likely related to their thermal instability in comparison to normal alkyl phenols (Zhang et al., 2016, 2019).

The CN distribution of the second most abundant O_1 class with DBE 5 typically ranges from CN 12 to 50 (Fig. 3g, h, and i) and shows a significantly higher abundance of the compounds with CN 27 (**VI-a**; C_{27}), 28 (**VI-b**; C_{28}), and 29 (**VI-c**; C_{29} ; Fig. S4). Such compounds are likely alkyl or isoprenoidyl phenols with a fused cycloalkane ring, and possibly derive from similar precursors and diagenetic pathways as the isoprenoidyl phenols, but are of uncertain origin yet (Liu et al., 2015).

The DBE distribution of the O_2 class in the Serra Alta shale (Fig. 5a) and Irati black shales from Amaral Machado and São Mateus do Sul (Fig. 5b and c) ranges from DBE 1 to 17, which likely encompasses carboxylic acids (Kim et al., 2005; Shi et al., 2010; Wan et al., 2017; Martins et al., 2017). In general, compounds with DBE 1 (**VIII**) dominate the O_2 class (see also the plots of DBE versus CN in Fig. S7), and are assigned as acyclic fatty acids (FA). A dominance of fatty acids among all carboxylic acids in the Irati pyrolysates (shale oil) has been already reported by Afonso et al. (1992b), and homologs up to nC_{36} were found in the Irati bitumen (Carvalhaes and Cardoso, 1986). Moreover, prominent compounds with DBE 5 (**IX**) and 6 (**X**; Fig. S7) are possible acidic biomarkers (cf. Lopes et al., 1999; Ji et al., 2018). These compounds likely correspond to naphthenic acids with four rings (e.g., steranoic acids;

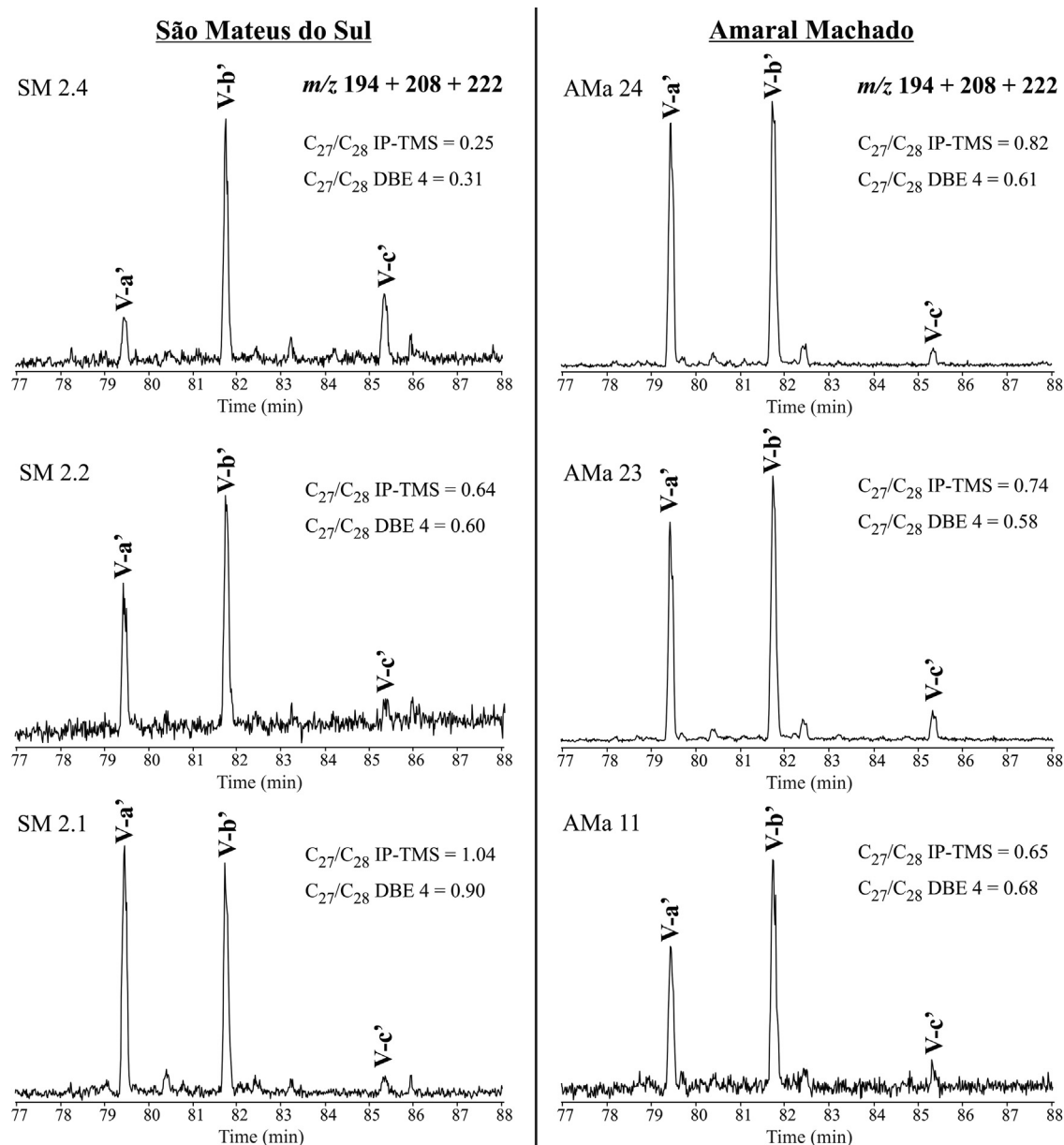


Fig. 4. Representative summed mass chromatograms m/z 194 + 208 + 222 showing the distribution of the methyl- (**V-a'**) and dimethyl isoprenoidyl phenols (**V-b'**) as trimethylsilyl ethers (TMS) in the NSO fraction of the Irati black shales treated with silylating reagent. The peaks labelled with **V-c'** are tentatively identified as trimethyl isoprenoidyl phenols-TMS. C_{27}/C_{28} DBE 4 of O₁ class based on their TMA from ESI(-) FT-ICR-MS analysis; C_{27}/C_{28} isoprenoidyl phenols as trimethylsilyl ethers (IP-TMS) based on their peak areas from GC-MS analysis.

Fasciotti et al., 2013) or benzoic acids, and naphthenic acids with five saturated rings (e.g., hopanoic acids; Farrimond et al., 2002; Shi et al., 2010) or 5,6,7,8-tetrahydronaphthalene carboxylic acids (Kim et al., 2005), respectively.

Fatty acids (DBE 1) that dominate the O₂ compounds range from CN 12 to 48 (Fig. 5d, e, and f). The acidic fraction of the Irati black shales is known to be composed of linear carboxylic acids rather than of the branched ones (Carvalhaes and Cardoso, 1986), which is in contrast to the dominance of isoprenoids (such as pristane or phytane over hydrocarbons; Martins et al., 2020a) typically found in immature sediments. Additionally, there is a marked predominance of even carbon-numbered fatty acids over those with odd carbon numbers. Using GC-MS analyses, Afonso et al. (1992b) have already shown this strong carbon preference in oil sourced from the Irati shale for the C₆-C₂₆ linear fatty acids as an indication of higher land plants. Such dominance of even carbon-

numbered fatty acids was also observed in data about several fossil organic mixtures gained by FT-ICR-MS (Wan et al., 2017; Ziegs et al., 2018b; Han et al., 2018a), and is in accordance with the characteristics of fatty acids in ancient and recent sediments (Tissot and Welte, 1984). The abundant O₂ compounds with DBE 1 and CN 16 likely correspond to hexadecanoic acid (**VIII-a**; C₁₆H₃₂O₂; cf. Shi et al., 2010; Liu et al., 2015; Han et al., 2018a). Alternative candidates for these DBE 1 compounds are other acyclic acids, however, ESI FT-ICR-MS data do not allow to differentiate between normal and branched fatty acids. Likely sources of such acids are land plants and algae (Cranwell, 1973; Bourbonniere and Meyers, 1996). The likely long-chained *n*-alkanoic acids with CN 24 (**VIII-b**), CN 26 (**VIII-c**), and CN 28 (**VIII-d**) also occur in the Irati Shale in higher abundance (Fig. 5e and f) and can be traced back to the waxy coatings of land plant leaves, flowers, spores, and pollen (Cranwell, 1973; Bourbonniere and Meyers, 1996).

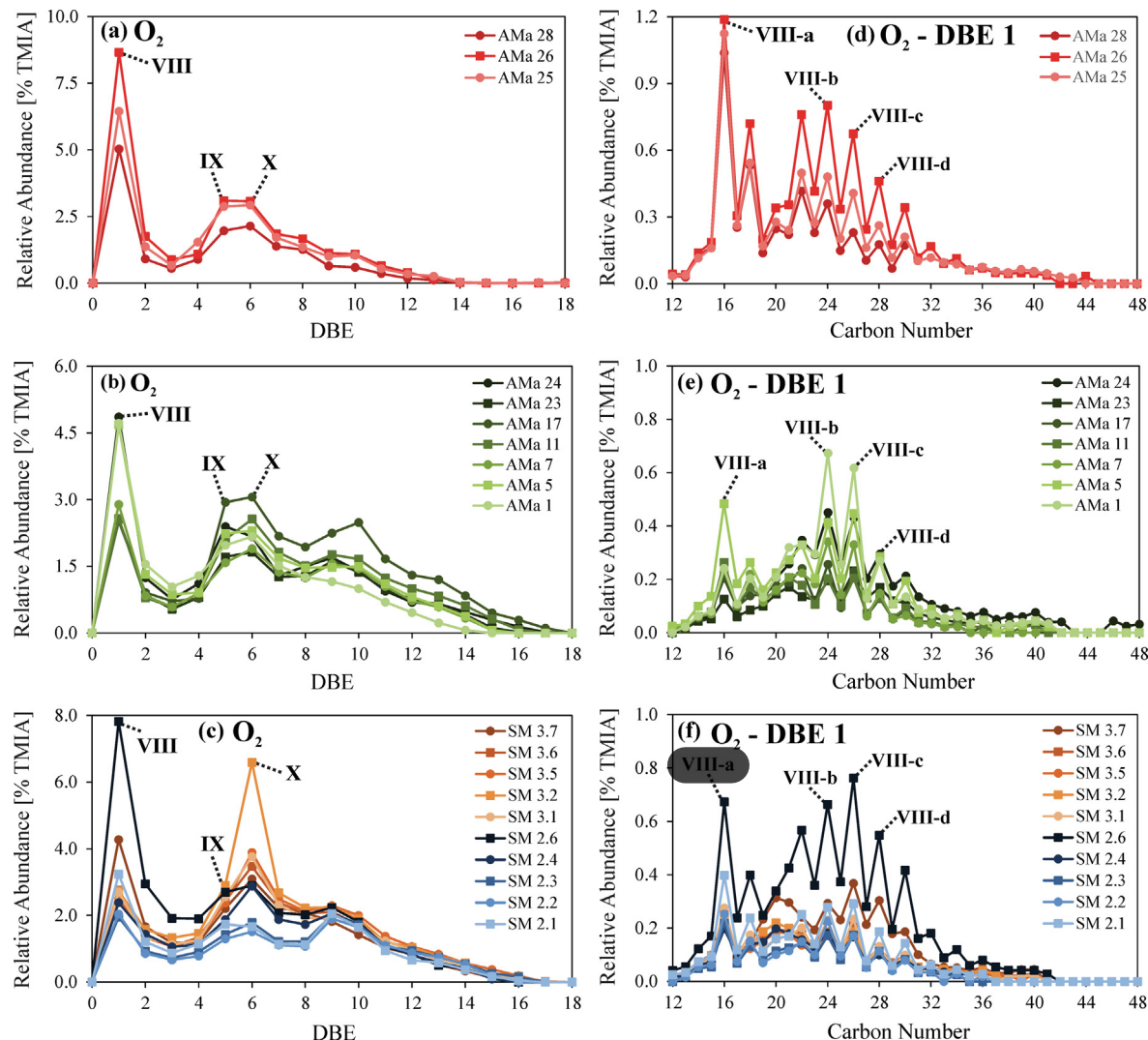


Fig. 5. DBE distribution of the O₂ class in the Serra Alta shale (a), and Iriti black shales from Amaral Machado (b) and São Mateus do Sul (c) areas. CN distribution for O₂ DBE 1 class in the Serra Alta shales (d), and Iriti black shales from Amaral Machado (e) and São Mateus do Sul (f) areas.

The presumable steranoic acids dominate the DBE 5 class of O₂ compounds mostly ranging from CN 27 to 31 (Fig. 6a, b, and c; Fig. S7; whole CN distribution ranging from 13 to ~47), with the highest abundance of CN 28 (IX-a); except for samples 3.2 with the highest abundance of CN 30 (IX-b) and 30 (IX-c). Steranoic acids are known from immature sediments (Schaeffer et al., 1993; Lopes et al., 1997, 1999; Fasciotti et al., 2013; Ajaero et al., 2016), and decarboxylate into steranes while thermal maturation proceeds (Poetz et al., 2014). These results are in agreement with the higher abundance of C₂₇ steranes in the Iriti black shales (Martins et al., 2020a) likely originated from C₂₈ steranoic acids, and refer to a similar reaction pathway of C₂₈ and C₂₉ steranes probably originated from C₂₉ and C₃₀ steranoic acids, respectively.

The assumed hopanoic acids with CN between 28 and 32 dominate the O₂ DBE 6 class in all samples (Fig. 6d, e, and f; Fig. S7, whole CN distribution ranging from 13 to ~47), with general highest abundance of CN 31 (X-a) followed by compounds with CN 30 and 32. Hopanoic acids as potential precursors of hopanes are ubiquitous in immature sediments (e.g., Schaeffer et al., 1993; Bennet and Abbott, 1999; Farrimond et al., 2002). Therefore, our results serve as an explanation for the high abundance of hopanes in the Iriti black shales, which are dominated by C₃₀ hopanes

(Martins et al., 2020a, b) possibly originated from C₃₁ hopanoic acids, and also refers to the occurrence of C₂₉ and C₃₁ hopanes as diagenetic products of C₃₀ and C₃₂ hopanoic acids, respectively.

The DBE distribution of the S₁O₃ class ranges from DBE 0 to 10 and from 0 to 12 for the S₁O₄ class (Fig. S8). The S₁O₃ class encompasses naphthenic and monoaromatic compounds, such as benzenesulfonic acids (XI) and naphthalenesulfonic acids (XII) with various side chains (Tomczyk et al., 2001). These SO compounds are conversion products of marine organic matter in sediments deposited under anoxic conditions (Orr and Sinnighe Damsté, 1990; Hughey et al., 2002). The amount of these acids maximizes at the base of the Amaral Machado unit deposited in a hypersaline environment, and at the base of the lower profile in São Mateus do Sul which represents a mesosaline paleoenvironment (see also DBE vs. CN in the Fig. S9). These anaerobically oxidized sulfur compounds are highly sensitive against thermal overprint and readily degraded (Hughey et al., 2004), but occur in the investigated Iriti black shales due to their low thermal maturity. S₁O₃ and S₁O₄ compounds with a similar DBE range from 0 to 9 were also found in oils of the Upper Jurassic Smackover Formation (Hughey et al., 2004). Here, a similar pattern for the S₁O₄ class DBE distribution with the compounds with DBE 1 (XIII) and 4 (XIV) occurs.

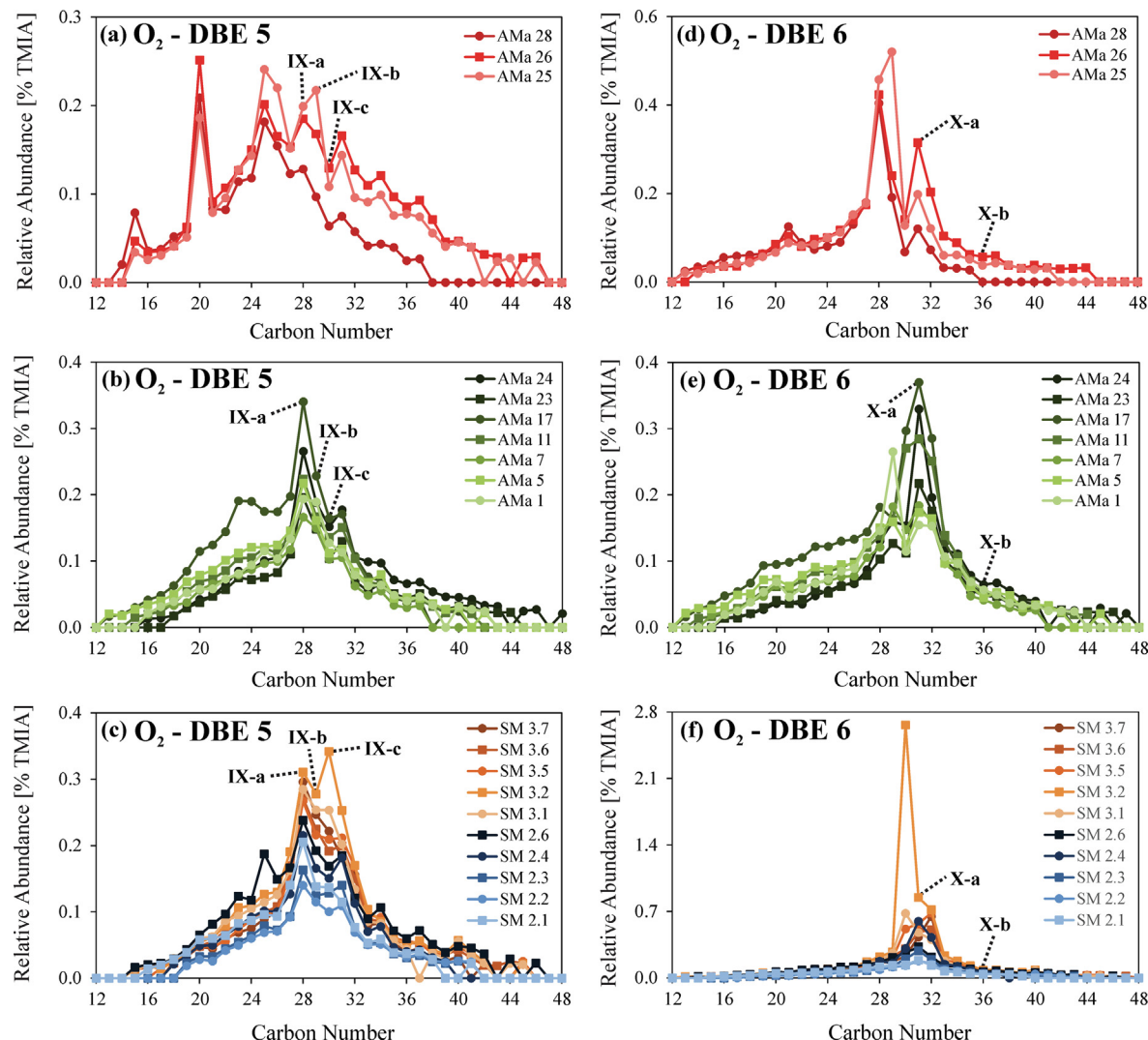


Fig. 6. CN distribution for O_2 DBE 5 and 6 classes in the Serra Alta shale (a and d), and Irati black shales from Amaral Machado (b and e) and São Mateus do Sul (c and f) areas. O_2 compounds with DBE 5 and CN 28, 29, and 30 likely representing steranoic acids (IX-a; IX-b; IX-c) and with DBE 6 and CN 31 to 36 likely representing hopanoic acids (X-a to X-b).

4. Discussion

Previous conventional biomarker studies based on the analysis of hydrocarbons have shown that the herein investigated Irati black shale samples were deposited on the mobile southern margin of Gondwana in a marine setting with anoxic bottom water. The depletion in dissolved oxygen was a result of water stratification due to a denser marine bottom water overlain by a lighter, less saline freshwater sourced from the continent (Mello et al., 1993; Goldberg and Humayun, 2016; Reis et al., 2018; Martins et al., 2020a, b). The sediments have TOC contents between 4 and 22 wt%, and the organic matter type is a kerogen type I/II with hydrogen indexes (HI) ranging from 348 to 631 mg HC/g TOC (Table 1). However, the deposition was coupled to progressively increasing freshwater influxes into the Irati Sea. For example, the basal Irati black shales (AMa 1 and 5) from Amaral Machado (northeastern Paraná Basin) were deposited in a shallow marine environment with reducing and hypersaline conditions whereas most of the younger sediments have stored organic signals of deposition at greater water depth and lower salinity (Martins et al., 2020a, b). A similar result was gained by the investigation of the black shales from the São Mateus do Sul site. Here, a prevail-

ing marine mesosaline and restricted environment was progressively diluted together with increasing terrigenous organic matter input. The signals of progressive incorporation of land plant material are stored in the uppermost samples of the Amaral Machado profile (samples AMa 25, 26, and 28) which represent the overlying Serra Alta Formation. These samples, having low TOC contents between 0.28 and 0.45 wt% (Table 1), were deposited in dysoxic/oxic waters (Matos et al., 2017), and the mostly terrigenous organic matter is dominated by phytoclasts (Martins et al., 2020c). Such paleoenvironmental changes are reflected by the ESI (-) ultra-high resolution mass spectrometric data in the form of variations in the abundance of heteroatom classes (e.g., O_1 , O_2 , $O_{>2}$, N_1 , N_1O_x , N_2O_x , and S_1O_x). In the following, we will discuss the NSO data under the light of the aforementioned paleoenvironmental changes and will test their use as new proxies to assess such changes.

4.1. Maturity assessment by N_1 class characteristics

The distribution pattern of the ESI(-) accessible pyrrolic N_1 compounds offers the possibility to prove previous maturity estimations of source rocks and oils since these nitrogen-bearing

compounds develop toward larger, more aromatic compounds with increasing maturity (Poetz et al., 2014; Oldenburg et al., 2014). Ternary diagrams are commonly applied to evaluate maturity by plotting the relative distribution of selected N₁ DBE classes that represent fully aromatized pyrrolic compounds (Oldenburg et al., 2014; Poetz et al., 2014) such as carbazoles (**I**, DBE 9), benzocarbazoles (**II**, DBE 12), dibenzocarbazoles (**III**, DBE 15) and benzonaphthocarbazoles (**IV**, DBE 18). Based on Fig. S2 and plots of DBE versus CN of the N₁ compounds (Fig. S3) together with the results from Poetz et al. (2014), the ternary diagrams in Fig. S10 show that all the Irati black shales are classified as immature to marginally mature (R₀ up to 0.53%), with the basal samples from Amaral Machado (AMa 1, 5, 7, and 11) being more mature. These base samples from Amaral Machado contain less abundant N₁ compounds with DBE 9 compared to DBE 15 (Fig. S2a), which is indicative for aromatization and therefore a slightly higher maturity.

These findings are in agreement with previous results from the analysis of aliphatic and aromatic biomarkers that clearly demonstrated that these samples are immature, but also that samples from the base of Amaral Machado were thermally overprinted (Martins et al., 2020b). Maturation here was caused by heat effects of diabase sills which intruded in the Paraná Basin (the Serra Geral Formation; Sousa et al., 1997; Araújo et al., 2005), leading to a beginning oil generation (Martins et al., 2020c).

In summary, there are no great maturity differences in the investigated Irati black shale samples. Therefore, the prominent variations in the elemental and compound class distributions among the Irati black shales presented in Table 1 (also in Fig. S1) and Fig. 2 are clear indicators of changes in water salinity and organic matter input (Martins et al., 2020a, b).

4.2. Compositional variations of NSO classes as tracers for depositional environment and organic matter input

The O₁ class containing methylated isoprenoidyl phenols (**V**; alkylphenols derived from lignin of higher plants; Tulipani et al., 2015) relatively increases from the base to the top in the Irati black shales at the Amaral Machado site (Fig. 7a), reaching higher values for samples AMa 23 and 24 (see also Fig. 3b). However, the Irati black shales from the base of the lower unit in São Mateus do Sul show a decrease of the O₁ class abundance in the marine mesosaline zone toward the top, but an increase in the upper unit (Fig. 7b). In contrast, the O₂ class which is linked to the presence of carboxylic acids is less concentrated in the basal portions of both profiles (AMa 1, 5, and 7; SM 2.1, 2.2, and 2.3). It relates to a deposition in a hyper/mesosaline marine environment, and possibly also to more reducing conditions. The obviously higher abundance of both the O₂ and the O_{>2} classes in sample SM 2.6 (Figs. 2, 5c, and 7b) and in the Serra Alta Formation (samples AMa 25, 26, and 28; Figs. 2 and 7a) mirrors a re-oxygenation due to the influx of freshwater and/or the high input of terrestrial organic matter, and less marine productivity causing a markedly lower TOC content (4.55 wt% for sample SM 2.6 and between 0.28 and 0.45 wt% for samples AMa 25, 26, and 28; Table 1). These results are in accordance with their higher oxygen indexes (OI) obtained from Rock-Eval analysis (Table 1).

The abundance of the N₁ class is higher in the basal samples from the lower São Mateus do Sul unit (samples SM 2.1, 2.2, 2.3, and 2.4). This feature reflects a deposition in mesosaline marine environments, although microbial bloom events (likely *Botryococcus*) occurred during freshwater incursions (Martins et al., 2020a; Figs. 2 and 7). The markedly higher algal contribution to these samples was pointed out by Martins et al. (2020a) by their higher concentrations of the isoprenoids pristane and phytane, nC₁₇, and C₁₇ long-chain alkylnaphthalene. This is in accordance with Rocha

et al. (2018) who suggested that lacustrine freshwater oils tend to be enriched in N_x compounds, possibly due to great algal input. Basically, the precursors of these nitrogen compounds are supposed as amino acids of proteins in plankton and bacteria (Baxby et al., 1994). In addition, nitrogen also originates from chlorophyll and is usually found in source-rock bitumen and petroleum preserved in porphyrins (Baxby et al., 1994). The Serra Alta shales, however, only have few N₁ compounds due to their higher content of terrigenous organic matter as higher land plants are mostly composed of lignin and cellulose, and only a little protein. Nonetheless, their low abundance of N₁ compounds can also be related to the lower ionization response factor of pyrrolic compounds compared to carboxylic acids and phenols (Hughey et al., 2002; Liao et al., 2012; Corilo et al., 2013).

N₁O_x and N₂O_x compounds are also present in significant amounts in the Irati black shales, and their abundance increases toward the top of the Irati Formation (Fig. 7), and thus with the influx of freshwater during deposition. The Serra Alta shales, in contrast, have few of these compounds, which indicates that these compounds are not related to terrigenous organic matter input (Baxby et al., 1994).

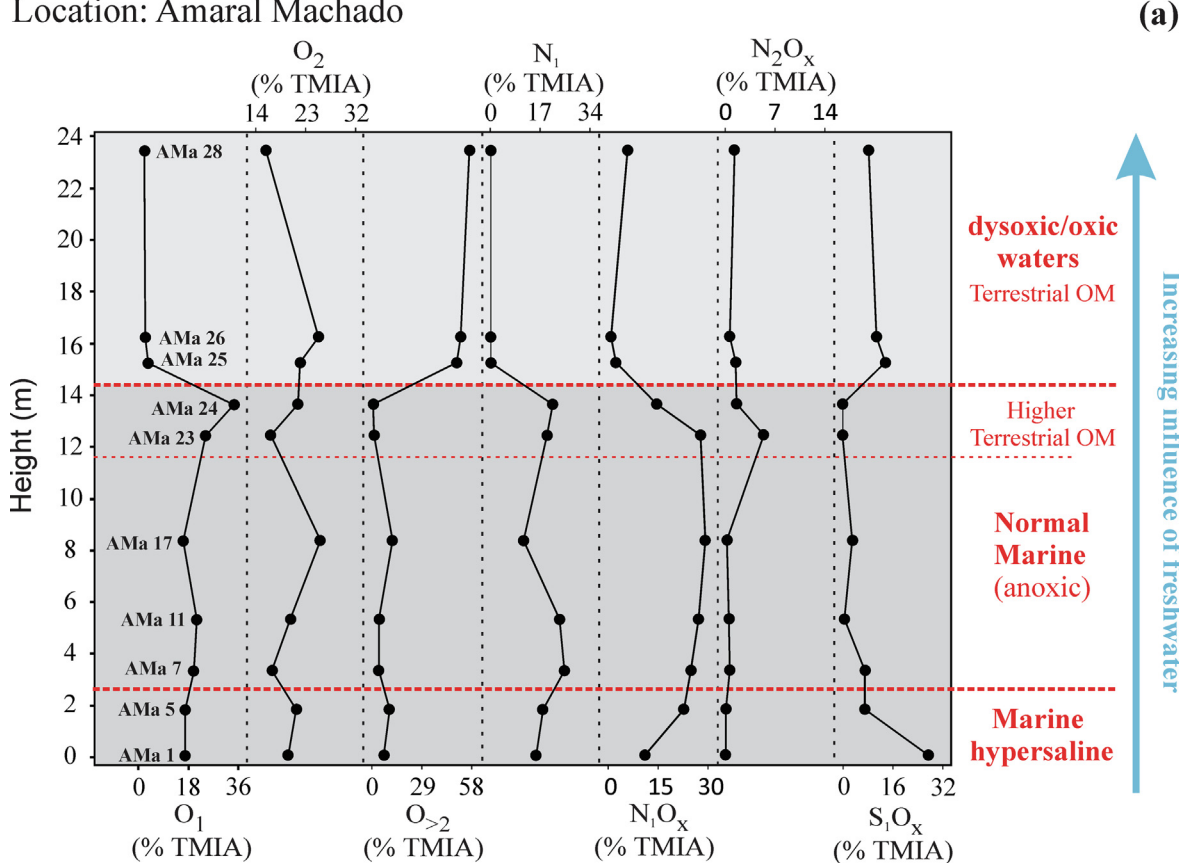
The S₁O_x class predominates in the basal Irati black shales deposited in a marine hypersaline environment (Fig. 7a; profile Amaral Machado), but decreases in the mesosaline or normal marine environment toward the top of the freshwater-influenced units (Fig. 7). These results corroborate the harsh depositional conditions for the samples AMa 1 and 5 when archaea and marine red algae flourished in an extreme sulfide-rich sea (Martins et al., 2020a). The sulfur compounds in the S₁O_x class were synthesized in the sediment either during early diagenesis (Wakeham et al., 1995; or even later during kerogen formation according to Hughey et al., 2002). These organic sulfur compounds are thus organic geochemical products of reactions with hydrogen sulfide or polysulfides generated during bacterial sulfate reduction with functionalized precursors (Kohnen et al., 1991; Rullkötter, 1993; Hughey et al., 2002).

4.3. New NSO parameters for paleoenvironmental reconstructions

Based on the distribution and variations of the acidic NSO compounds in the Irati black shales and Serra Alta shales, eight new parameters based on ESI(-) FT-ICR-MS data are suggested as new proxies to assess changes of the paleoenvironmental conditions (Fig. 8; calculation details in Table 2): phenol index (%DBE 4; O₁ class); C₂₇/C₂₈ DBE 4 (O₁ class); C₂₇/C₂₈ DBE 5 (O₁ class); Even/Odd_{FA}; TAR_{FA} Odd (TAR, terrigenous/aquatic ratio); and TAR_{FA} Even; C₃₆ hopanoic acid index; and hopanoic/steranoic acids ratio. Additionally, we also tested and applied the parameter OEP_{FA} proposed by Wang and Zhu (2019; Fig. 8, Table 2). In general, all parameters reflect the changes of the paleoenvironment during the deposition of the Irati black shales (Fig. 8, compare with signatures of depositional environment on the right-hand side; after Martins et al., 2019, 2020a, b, c). These changes are more pronounced in the Amaral Machado and lower São Mateus do Sul units (Fig. 8), implying dynamic paleoenvironmental conditions controlled by increasing freshwater influxes, while the parameters in the upper São Mateus do Sul unit remain fairly constant due to the prevailing brackish water environment (Martins et al., 2020a). All parameter values correlate well with variations of hydrocarbon biomarker parameters and their meaning (Martins et al., 2020a, b).

In general, an increasing %DBE 4 (O₁ class; phenol index) represents the increasing amount of alkylphenols possibly from higher plants (Ioppolo-Armanios et al., 1993; Tulipani et al., 2015). A similar tendency is also visible in the Irati units, mainly in the Amaral Machado profile with phenol index increasing toward the top of

Location: Amaral Machado



Location: São Mateus do Sul

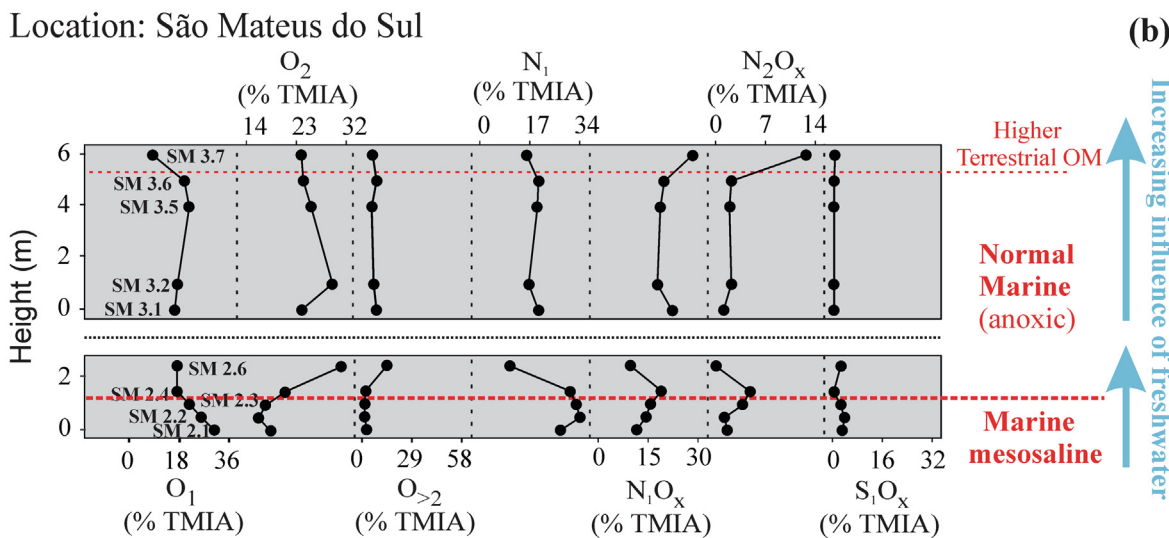


Fig. 7. Variations of the heteroatom O₁, O₂, O_{>2}, N₁, N₁O_x, N₂O_x, S₁O_x classes dependent on changes in the depositional environment conditions during deposition of the Irati black shales and Serra Alta shales (according to Martins et al., 2020a, b, c), from both Amaral Machado (a) and São Mateus do Sul (b) areas.

the unit (Fig. 8a), and is based on a pronounced run-off and transport of higher land plant material. A further observation supports this enrichment of O₁ compounds with 4 DBE: it is their occurrence in crude oils generated from lacustrine source rocks (Rocha et al., 2018, 2019). It is important to note that the high phenol index for sample SM 2.1 (Fig. 8b) is in agreement with its higher concentration of pristane, phytane, nC₁₅, nC₁₇, and aliphatic carotenoids all from freshwater algae (Martins et al., 2020a).

The ratios between the most abundant DBE 4 and 5 O₁ compounds with 27 and 28 CN (C₂₇/C₂₈ DBE 4 and C₂₇/C₂₈ DBE 5), sug-

gested here for the first time, decrease continuously toward the top of all Irati Shale units (Fig. 8). The compounds behind are methylated isoprenoidyl phenols, which are structurally similar to and have a possibly similar biosynthetic pathway as methylated methyltrimethyltridecylchromans (MTTCs) (Barakat, and Rullkötter, 1997) that were identified previously in these Irati black shale samples. The MTTCs occur preferentially as methylated rather than as dimethylated compounds (C₂₇H₄₆O and C₂₈H₄₈O, respectively) in the basal samples deposited under high salinities (Martins et al., 2020a). This preference also is observed for the

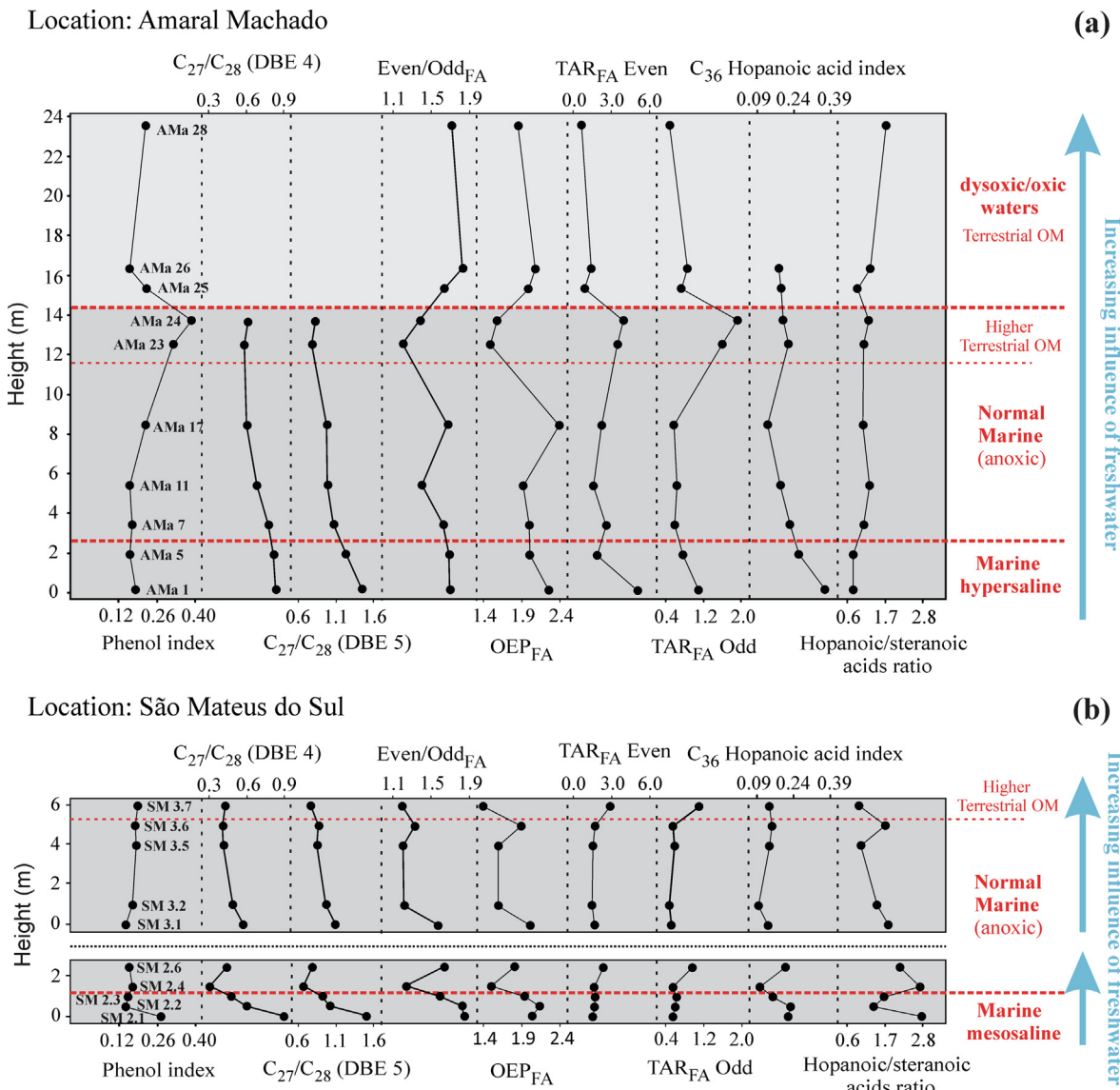


Fig. 8. Variations of the new parameters to assess changes of the depositional environment of the Irati black shales and Serra Alta shales (classification according to Martins et al., 2020a, b, c), from both Amaral Machado (a) and São Mateus do Sul (b) areas. Calculation procedures are presented in Table 2.

methylated isoprenoidyl phenols in the basal samples as for the higher content of O₁ compounds with 27 rather than with 28 CN (DBE 4 and 5; Fig. 3). The pattern of the C₂₇/C₂₈ (DBE 4) ratio resembles that of the C₂₇/C₂₈ (DBE 5) ratio, pointing to a similar origin and/or interrelated controls. Moreover, both ratios positively correlate with the ratio between Me-MTTC and diMe-MTTCs (compound assessment by GC-MS; Fig. 9). In conclusion, higher values of the C₂₇/C₂₈ DBE 4 and C₂₇/C₂₈ DBE 5 ratios develop with increasing salinity and can be used for paleosalinity studies. Additionally, their decrease plotted along a stratigraphic profile may indicate an influx of freshwater when calibrated against marine average conditions.

The O₂ compounds with DBE 1 are acyclic fatty acids that are the most abundant lipid markers for marine phytoplankton, here mainly microalgae, and also zooplankton, terrestrial higher plants, and bacteria (Liu and Liu, 2016; Rao et al., 2016). The higher %DBE 1 (O₂ class; Fig. 5) in samples from the base of the units and its decrease toward the top of the units points to the origin of fatty acids from marine microalgae since the bottom samples from both localities (AMa 1 and 5, and SM 2.1, 2.2, and 2.3) are marine sedi-

ments (Martins et al., 2020a). Additionally, samples from the top of the units (AMa 23 and 24, SM 2.6, and 3.7) with pronounced freshwater characteristics and a higher content of terrestrial organic matter also have higher fatty acid abundance, finally indicators for fatty acids from terrestrial higher plants, mainly linear carboxylic acids with CN 24 (VIII-b), 26 (VIII-c), and 28 (VIII-d). The samples with a higher abundance of DBE 1 O₂ compounds also reflect higher concentrations of n-alkanes (nC₁₂ to nC₃₆, from GC-FID analysis; Fig. S11). With the end of the black shale sedimentation, the fatty acids in the Serra Alta shales (Fig. 5a and d) indicate dominantly diagenetic products from higher land plant material (phytoclasts; Martins et al., 2020c).

The observed even-to-odd predominance of fatty acids in the investigated shales reflects their low maturity, however, its variation among the samples is associated with changes of the organic matter source. An even-to-odd predominance of fatty acids generates an odd-to-even predominance of n-alkanes (Tissot and Welte, 1984; Wan et al., 2017) since these linear acids are converted to n-alkanes by decarboxylation already during early diagenesis and later during the thermal evolution of the source rock. The Even/

Table 2

Overview of FT-ICR-MS derived diagnostic ratios with name, input parameters, and reference.

Diagnostic ratio	Input parameters	Reference
Phenol index [%DBE 4 (O ₁ class)]	DBE 4 of O ₁ class TMIA over total O ₁ class TMIA	Based on Rocha et al. (2019)
C ₂₇ /C ₂₈ (DBE 4)	C27 from DBE 4 of O ₁ class TMIA over C28 from DBE 4 of O ₁ class TMIA	Herein
C ₂₇ /C ₂₈ (DBE 5)	C27 from DBE 5 of O ₁ class TMIA over C28 from DBE 5 of O ₁ class TMIA	Herein
Even/Odd _{FA}	Even C20 to C36 from DBE 1 of O ₂ class TMIA over odd C19 to C35 from DBE 1 of O ₂ class TMIA	Herein
OEP _{FA}	C22 plus 6*C24 plus C26 from DBE 1 of O ₂ class TMIA over 4*C23 plus 4*C25 from DBE 1 of O ₂ class TMIA	Wang and Zhu (2019)
TAR _{FA} Even	Sum of C24, C26, and C28 from DBE 1 of O ₂ class TMIA over sum of C12, C14, and C16 from DBE 1 of O ₂ class TMIA	Based on Bourbonniere and Meyers (1996)
TAR _{FA} Odd	Sum of C27, C29, and C31 from DBE 1 of O ₂ class TMIA over sum of C15, C17, and C19 from DBE 1 of O ₂ class TMIA	Based on Bourbonniere and Meyers (1996)
C ₃₆ Hopanoic acid index	C36 from DBE 6 of O ₂ class TMIA over C31 from DBE 6 of O ₂ class TMIA	Herein
Hopanoic/steranoic acids ratio	C31 from DBE 6 of O ₂ class TMIA over C28 from DBE 5 of O ₂ class TMIA	Herein

* TMIA: Total Monoisotopic Ion Abundance.

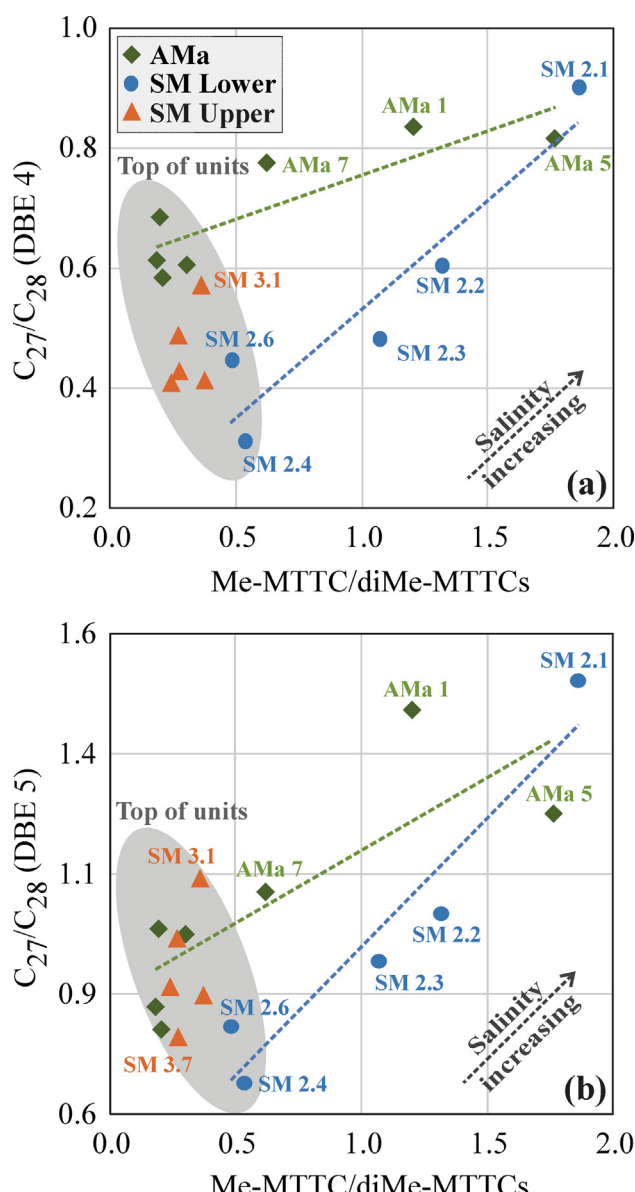


Fig. 9. Plots of the Me-MTTC/diMe-MTTCs ratio obtained from GC-MS analysis against C₂₇/C₂₈ (DBE 4; a) and C₂₇/C₂₈ (DBE 5; b) obtained from ESI(-) FT-ICR-MS analysis of the Irati black shales. The salinity trends are highlighted by dotted arrows. AMa: Amaral Machado Quarry; SM Upper and Lower: upper and lower units of São Mateus do Sul Quarry.

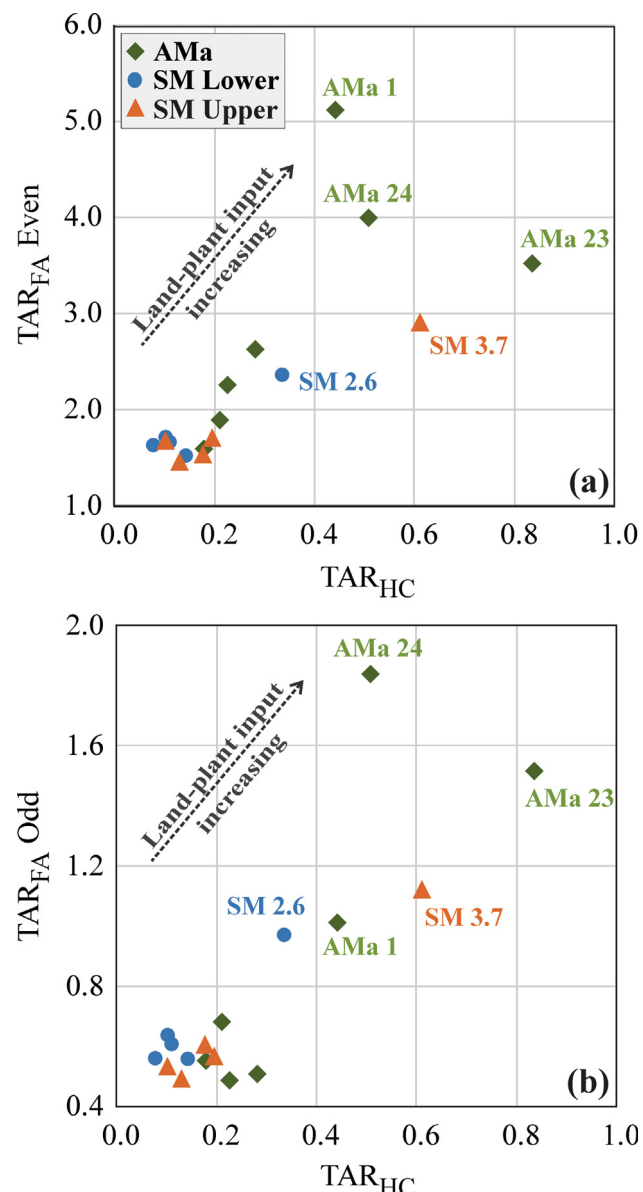


Fig. 10. Plots of the TAR_{HC} obtained from GC-FID analysis against TAR_{FA} Even (a) and TAR_{FA} Odd (b) obtained from ESI(-) FT-ICR-MS analysis of the Irati black shales (class O₂, DBE 1). Dotted arrows indicate land-plant input trends. AMa: Amaral Machado Quarry; SM Upper and Lower: upper and lower units of São Mateus do Sul Quarry.

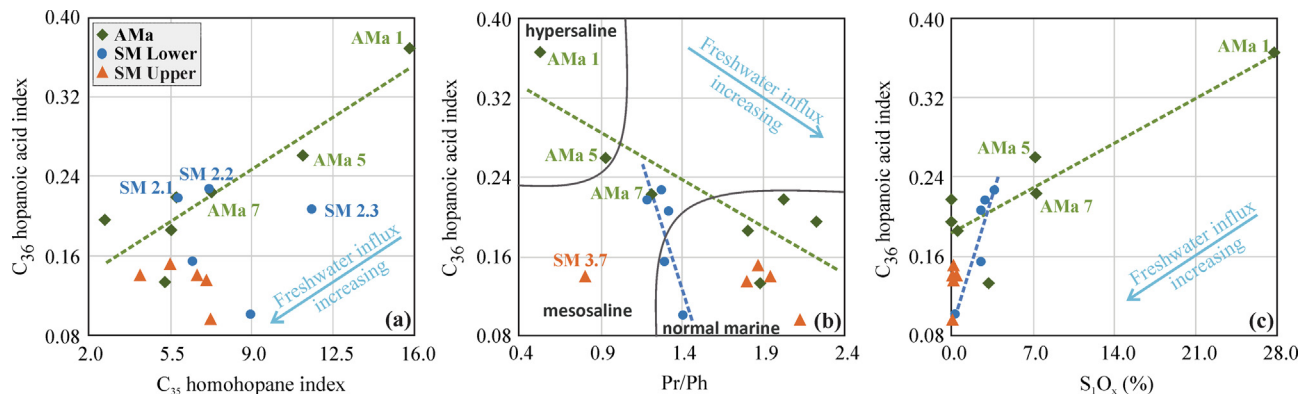


Fig. 11. Plots of the C₃₆ hopanoic acid index suggested in this work against the C₃₅ homohopane index (a) obtained from GC-MS analysis and Pr/Ph (pristane over phytane; b) obtained from GC-FID (Martins et al., 2020a), and S₁O_x (c) from the ESI(-) FT-ICR-MS analysis. The freshwater influx trends are depicted by the light blue arrows, contrary to the salinity trends. AMa: Amaral Machado Quarry; SM Upper and Lower: upper and lower units of São Mateus do Sul Quarry. (For interpretation of the references to colour in this figure legend, the reader is referred to the web version of this article.)

Odd_{FA} and OEP_{FA} are generally higher in the Irati black shales in the Amaral Machado profile (Fig. 8a) as a reflection of the higher content of terrigenous organic matter at this site, which was a shallow and more proximal depositional setting (Martins et al., 2020b). Moreover, also the Serra Alta shales present high values of the parameters Even/Odd_{FA} and OEP_{FA}, in accordance with a great input of land plants (Martins et al., 2020c). In order to quantify the different portions of organic matter mixtures by using fatty acids, the TAR_{FA} parameter was calculated according to Bourbonniere and Meyers (1996). This parameter includes quantities of the long and straight-chained C₂₄, C₂₆, and C₂₈ fatty acids with high molecular weights that are dominant components of the waxy coatings of higher plant leaves and pollens (Riley et al., 1991; Duan et al., 1997), while short-chained C₁₂, C₁₄, and C₁₆ fatty acids occur in all plants and are also dominant lipid components of algae (Cranwell, 1973). The TAR_{FA} Even values are generally higher in Irati black shales from the Amaral Machado unit (Fig. 8a) with its higher content of terrigenous organic matter due to its more proximal setting and corresponding characteristics, and their values are also higher for samples at top of both units (AMa 23 and 24, SM 2.6 and 3.7; Martins et al., 2020b). Such values are even higher in samples AMa 1 and 5 likely due to the more continental influence. In addition, the pattern of the TAR_{FA} Even resembles that of the TAR_{FA} Odd, which indicates the same origin for even and odd fatty acids with similar number of carbon atoms.

Both ratios TAR_{FA} Even and TAR_{FA} Odd positively correlate with the TAR_{HC} (Fig. 10; from Martins et al., 2020b) that was calculated using the sum of the n-alkanes C₂₇ and C₂₉ (both originated from epicuticular waxes of land-plants) over the n-alkanes C₁₅, C₁₇, and C₁₉ originated from algae (assessed by GC-MS; Bourbonniere and Meyers, 1996). The observed good correlation between TAR_{FA} Even and the TAR_{HC} ratios (Fig. 10a) highlighted by their higher values of the samples AMa 1, 23, 24, and SM 3.7 verifies the genetic relationship between the n-alkanes and their fatty acid precursors, insofar as linear acids are converted to n-alkanes during diagenesis and further thermal evolution (Kunst and Samuels, 2003; Wan et al., 2017).

Based on the CN distribution of the presumable steranoic (**IX**; DBE 5, class O₂) and hopanoic acids (**X**; DBE 6, O₂ class), and their known decarboxylation to generate steranes and hopanes (Farrimond et al., 2002), the C₃₆ hopanoic acid index and the hopanoic/steranoic acids ratio proposed in this work improve the assessment of the changes in the depositional paleoenvironment of the Irati black shales by polar compounds (Fig. 8). The C₃₆ hopanoic acid index trends resemble the C₃₅ homohopane index for the Irati black shales from the Amaral Machado unit (Fig. 11a; Martins

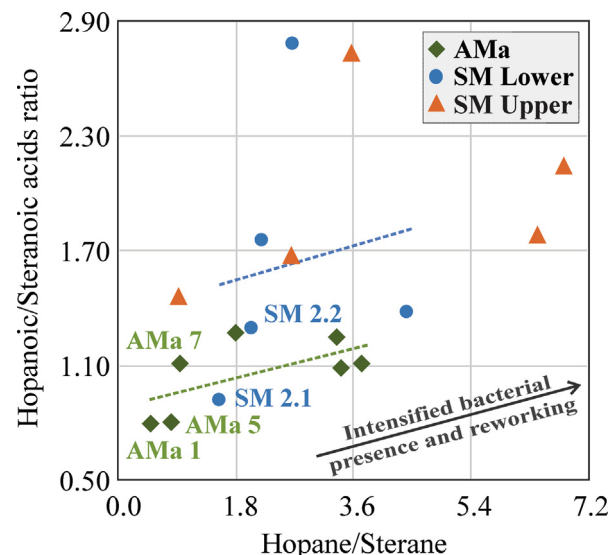


Fig. 12. Plot of the Hopanoic/Steranoic acids ratio suggested in this work against the Hopane/Sterane ratio obtained from GC-MS analysis (Martins et al., 2020a). Bacterial presence and reworking trends are given by the gray arrow. AMa: Amaral Machado Quarry; SM Upper and Lower: upper and lower units of São Mateus do Sul Quarry.

et al., 2020a). Both indexes are higher for the marine hypersaline basal samples (AMa 1 and 5) with lower Pr/Ph values (Fig. 11b), and also present high values for the basal samples from the lower São Mateus do Sul unit (SM 2.1, 2.2, and 2.3) deposited in a mesosaline environment (Fig. 11b), and decrease toward the top units. High values of the C₃₆ hopanoic acid index can thus indicate anoxic conditions in a highly reducing marine environment together with the C₃₅ homohopane index (Peters and Moldowan, 1991). This index also correlates with the percentage of S₁O_x compounds (see higher values to samples AMa 1, 5, and 7; Fig. 11c), and its increase along a stratigraphic profile might indicate an influx of freshwater. The hopanoic/steranoic acids ratio trends also resemble the hopane/sterane ratio for the Irati black shales (Fig. 12; Martins et al., 2020a) with lower values for the basal samples from the Amaral Machado unit (AMa 1 and 5), and with generally higher values for samples from the São Mateus do Sul units pointing to significant bacterial activity (Brassell et al., 1986) in anoxic bottom water or in photic euxinia zones (Martins et al., 2020a).

5. Conclusions and outlook

The spatial changes of the acidic NSO compound composition in the Irati black shales reflect the dynamics of this particular marine depositional environment on the post-glacial southern margin of Gondwana during the Early Permian that was influenced by a variable continental run-off and organic matter input. A major environmental break is also reflected by the NSO compounds when the younger Serra Alta shales were deposited. It becomes obvious that selective NSO signals are good proxies of salinity variations and different organic matter, and that these interfering signals can be deciphered by a wide range of established and new NSO proxies. Their application allows to semi-quantitatively estimate productivities of different biota and also the intensity of the bacterial reworking.

Here, higher values of phenol index and terrigenous/aquatic ratio based on fatty acids (TAR_{FA} Odd and Even) indicate higher land-plant input likely linked to the influx of freshwater as it is the even-to-odd predominance of fatty acids (higher Even/Odd_{FA}), while higher values of C₂₇/C₂₈ DBE 4 (methylated isoprenoidyl phenols; O₁ class) and C₂₇/C₂₈ DBE 5 (O₁ class) point to higher salinity. Additionally, a higher C₃₆ hopanoic acid index indicates a highly reducing marine environment, while a significant bacterial biomass signal is stored as a higher hopanoic/steranoic acids ratio.

NSO compounds and ratios thus offer the possibility to retrace processes of the depositional environment, especially in immature sediments. When calibrated against “classical” hydrocarbon biomarkers, the introduced new NSO proxies have the potential to unravel the influence of different water salinities and organic matter changes in dynamic depositional systems, e.g., on continental margins after glacial events as presented here. Other applications may be the analysis of the young geological history of marginal seas, as for example the Baltic Sea or Black Sea, or the analysis of extreme environments such as hypersaline settings or extreme sulfide-rich seas.

Other applications may be the analysis of the young geological history of marginal seas, as for example the Baltic Sea or Black Sea, or the analysis of extreme environments such as hypersaline settings or extreme sulfide-rich seas.

Declaration of Competing Interest

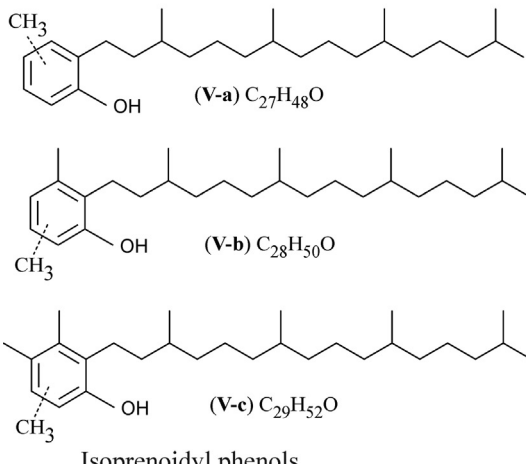
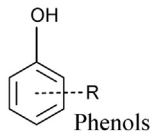
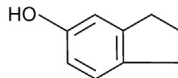
The authors declare that they have no known competing financial interests or personal relationships that could have appeared to influence the work reported in this paper.

Acknowledgments

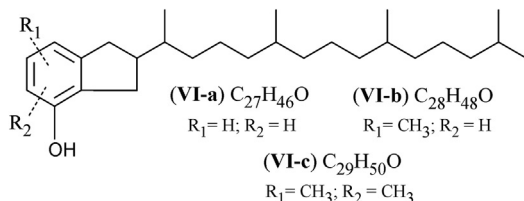
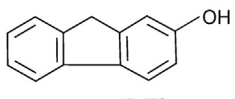
This work was supported by GFZ German Research Centre for Geosciences (Potsdam, Germany) and by North Fluminense State University – UENF (Macaé, Brazil). The authors thank GFZ staff for all support, especially Cornelia Karger. The authors express their appreciation to BG E&P Brasil Ltda., a current subsidiary of Shell Brasil Petróleo Ltda., for funding the field trip for sampling, which was made possible on behalf of the “Commitment to Research and Development Investments” along with the ANP (National Agency of Petroleum, Natural Gas and Biofuels) established on an application of resources (clause of R&D contracts in the Exploration and Production of Petroleum in Brazil). The authors also thank the Associate Editor Clifford C. Walters, and two anonymous reviewers for their important comments that improved the quality of this manuscript.

Appendix A

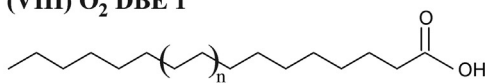
Examples of plausible structures of acidic O_x compounds according to the heteroatom composition, DBE, and carbon number (CN).

(V) O₁ DBE 4**(VI) O₁ DBE 5**

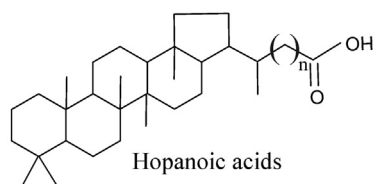
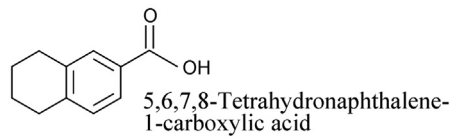
5-Indanol

**(VII) O₁ DBE 9**

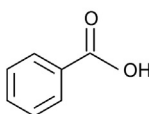
2-Fluorenol

(VIII) O₂ DBE 1

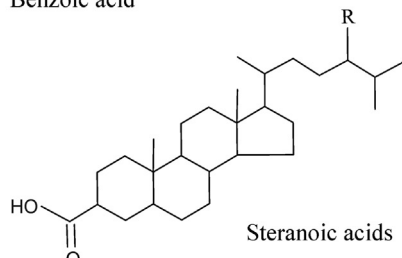
- (VIII-a) nC₁₆ Fatty acid (FA; n = 1)
(VIII-b) nC₂₄ Fatty acid (FA; n = 5)
(VIII-c) nC₂₆ Fatty acid (FA; n = 6)
(VIII-d) nC₂₈ Fatty acid (FA; n = 7)

(X) O₂ DBE 6

- (X-a) C₃₁ Hopanoic acid (n = 1)
(X-b) C₃₆ Hopanoic acid (n = 6)

(IX) O₂ DBE 5

Benzoic acid



Steranoic acids

- (IX-a) C₂₈ Steranoic acid (R = H)
(IX-b) C₂₉ Steranoic acid (R = CH₃)
(IX-c) C₃₀ Steranoic acid (R = C₂H₅)

Appendix B. Supplementary material

Supplementary data to this article can be found online at <https://doi.org/10.1016/j.orggeochem.2020.104152>.

Associate Editor—Clifford C. Walters

References

- Afonso, J.C., Cardoso, J.N., Schmal, M., 1992a. Distribution and origin of organic sulphur compounds in Iriti shale oil. *Fuel* 71, 409–415.
- Afonso, J.C., Schmal, M., Cardoso, J.N., 1992b. Acidic oxygen compounds in the Iriti shale oil. *Industrial & Engineering Chemistry Research* 31, 1045–1050.
- Ajero, C., Headley, J.V., Peru, K.M., McMurtin, D.W., 2016. Forensic studies of naphthenic acids fraction compounds in oil sands environmental samples and crude oil. In: Stout, S.A., Wang, Z. (Eds.), *Standard handbook oil spill environmental forensics*. Academic Press, pp. 343–397.
- Aráujo, C.C., Yamamoto, J.K., Rostirolla, S.P., Madrucci, V., Tankard, A., 2005. Tar sandstones in the Paraná Basin of Brazil: Structural and magmatic controls of hydrocarbon charge. *Marine and Petroleum Geology* 22, 671–685.
- Aráujo, L.M., Triguis, J.A., Cerqueira, J.R., Freitas, L.C. da S., 2000. The atypical Permian Petroleum System of the Paraná Basin, Brazil. In: Mello, M.R., Katz, B.J. (Eds.), *Petroleum Systems of South Atlantic margins*. AAPG Memoir 73, pp. 377–402.
- Bennet, B., Abbott, G.D., 1999. A natural pyrolysis experiment – hopanes from hopanoic acids? *Organic Geochemistry* 30, 1509–1516.
- Borisov, R.S., Kulikova, L.N., Zaikin, V.G., 2019. Mass spectrometry in petroleum chemistry (petroleomics) (review). *Petroleum Chemistry* 59, 1055–1076.
- Barakat, A.O., Baumgart, S., Brocks, P., Scholz-Bottcher, B.M., Rullkötter, J., 2012. Alkylated phenol series in lacustrine black shales from the Nördlinger Ries, southern Germany. *Journal of Mass Spectrometry* 47, 987–994.
- Barakat, A., Rullkötter, J., 1997. A comparative study of molecular paleosalinity indicators: chromans, tocopherols and C_{20} isoprenoid thiophenes in Miocene lake sediments (Nördlinger Ries, southern Germany). *Aquatic Geochemistry* 3, 169–190.
- Baxby, M., Patience, R.L., Bartle, K.D., 1994. The origin and diagenesis of sedimentary organic nitrogen. *Journal of Petroleum Geology* 17, 211–230.
- Blumer, M., 1957. Removal of elemental sulfur from hydrocarbon fractions. *Analytical Chemistry* 29, 1039–1041.
- Bourbonniere, R.A., Meyers, P.A., 1996. Sedimentary geolipid records of historical changes in the watersheds and productivities of Lakes Ontario and Erie. *Limnology and Oceanography* 41, 352–359.
- Brassell, S.C., Eglinton, G., Mo, F.J., 1986. Biological marker compounds as indicators of the depositional history of the Maoming oil shale. *Organic Geochemistry* 10, 927–941.
- Carvalhaes, S.F., Cardoso, J.N., 1986. Carboxylic acids in the shales of Iriti Formation. *Anais da Academia Brasileira de Ciências* 58, 7–15.
- Clegg, H., Wilkes, H., Horsfield, B., 1997. Carbazole distributions in carbonate and clastic source rocks. *Geochimica et Cosmochimica Acta* 61, 5335–5345.
- Corilo, Y.E., Podgorski, D.C., McKenna, A.M., Lemkau, K.L., Reddy, C.M., Marshall, A.G., Rodgers, R.P., 2013. Oil spill source identification by principal component analysis of electrospray ionization Fourier transform ion cyclotron resonance mass spectra. *Analytical Chemistry* 85, 9064–9069.
- Correa da Silva, Z.C., Cornford, C., 1985. The kerogen type, depositional environment and maturity, of the Iriti Shale, Upper Permian of Paraná Basin, Southern Brazil. *Organic Geochemistry* 8, 399–411.
- Cranwell, P.A., 1973. Chain-length distribution of n -alkanes from lake sediments in relation to post-glacial environmental change. *Freshwater Biology* 3, 259–265.
- Duan, Y., Wen, Q., Zheng, G., Luo, B., Ma, L., 1997. Isotopic composition and probable origin of individual fatty acids in modern sediments from Ruoguai Marsh and Nansha Sea, China. *Organic Geochemistry* 27, 583–589.
- Farrimond, P., Griffiths, T., Evdokiadis, E., 2002. Hopanoic acids in Mesozoic sedimentary rocks: their origin and relationship with hopanes. *Organic Geochemistry* 33, 965–977.
- Fasciotti, M., Lalli, P.M., Heerdt, G., Steffen, R.A., Corilo, Y.E., de Sá, G.F., Daroda, R.J., Reis, F.A.M., Morgan, N.H., Pereira, R.C.L., Eberlin, M.N., Klitzke, C.F., 2013. Structure-drift time relationship in ion mobility mass spectrometry. *International Journal for Ion Mobility Spectrometry* 16, 117–132.
- Faure, K., Cole, D., 1999. Geochemical evidence for lacustrine microbial blooms in the vast Permian Main Karoo, Paraná, Falkland Islands and Huab basins of southwestern Gondwana. *Palaeogeography, Palaeoclimatology, Palaeoecology* 152, 189–213.
- Goldberg, K., Humayun, M., 2016. Geochemical paleoredox indicators in organic-rich shales of the Iriti Formation, Permian of the Paraná Basin, southern Brazil. *Brazilian Journal of Geology* 46, 377–393.
- Han, Y., Poetz, S., Mahlstadt, N., Karger, C., Horsfield, B., 2018a. Fractionation and origin of NyOx and Ox compounds in the Barnett Shale sequence of the Marathon 1 Mesquite well, Texas. *Marine and Petroleum Geology* 97, 517–524.
- Han, Y., Poetz, S., Mahlstadt, N., Karger, C., Horsfield, B., 2018b. Fractionation of pyrrolic nitrogen compounds during primary migration of petroleum within the Barnett shale sequence of Marathon 1 Mesquite well, Texas. *Energy & Fuels* 32, 4638–4650.
- Hosseini, S.H., Horsfield, B., Poetz, S., Wilkes, H., Yalçın, M.N., Kavak, O., 2017. Role of maturity in controlling the composition of solid bitumens in veins and vugs from SE Turkey as revealed by conventional and advanced geochemical tools. *Energy & Fuels* 31, 2398–2413.
- Hughey, C.A., Rodgers, R.P., Marshall, A.G., Walters, C.C., Qian, K., Mankiewicz, P., 2004. Acidic and neutral polar NSO compounds in Smackover oils of different thermal maturity revealed by electrospray high field Fourier transform ion cyclotron resonance mass spectrometry. *Organic Geochemistry* 35, 863–880.
- Hughey, C.A., Rodgers, R.P., Marshall, A.G., Qian, K., Robbins, W.K., 2002. Identification of acidic NSO compounds in crude oils of different geochemical origins by negative ion electrospray Fourier transform ion cyclotron resonance mass spectrometry. *Organic Geochemistry* 33, 743–759.
- Ioppolo-Armanios, M., Alexander, R., Kagi, R.I., 1993. Identification and origins of isopropylmethylphenols in crude oils. *Organic Geochemistry* 22, 815–823.
- Ji, H., Li, S., Greenwood, P., Zhang, H., Pang, X., Xu, T., He, N., Shi, Q., 2018. Geochanical characteristics and significance of heteroatom compounds in lacustrine oils of the Dongpu Depression (Bohai Bay Basin, China) by negative ion Fourier transform ion cyclotron resonance mass spectrometry. *Marine and Petroleum Geology* 97, 568–591.
- Kim, S., Stanford, L.A., Rodgers, R.P., Marshall, A.G., Walters, C.C., Qian, K., Wenger, L.M., Mankiewicz, P., 2005. Microbial alteration of the acidic and neutral polar NSO compounds revealed by Fourier transform ion cyclotron resonance mass spectrometry. *Organic Geochemistry* 36, 1117–1134.
- Kohnen, M.E.L., Sinnighe Damsté, J.S., Ten Haven, H.L., Kock-Van Dalen, A.C., Schouten, S., de Leeuw, J.W., 1991. Identification and geochemical significance of cyclic di- and trisulfides with linear and acyclic isoprenoid carbon skeletons in immature sediments. *Geochimica et Cosmochimica Acta* 55, 3685–3695.
- Kunst, L., Samuels, A.L., 2003. Biosynthesis and secretion of plant cuticular wax. *Progress in Lipid Research* 42, 51–80.
- Liao, Y., Shi, Q., Hsu, C.S., Pan, Y., Zhang, Y., 2012. Distribution of acids and nitrogen containing compounds in biodegraded oils of the Liaohe Basin by negative ion ESI FT-ICR MS. *Organic Geochemistry* 47, 51–65.
- Liu, H., Liu, W., 2016. n -Alkane distributions and concentrations in algae, submerged plants and terrestrial plants from the Qinghai-Tibetan Plateau. *Organic Geochemistry* 99, 10–22.
- Liu, P., Li, M., Jiang, Q., Cao, T., Sun, Y., 2015. Effect of secondary oil migration distance on composition of acidic NSO compounds in crude oils determined by negative-ion electrospray Fourier transform ion cyclotron resonance mass spectrometry. *Organic Geochemistry* 78, 23–31.
- Lopes, J.A.D., Santos Neto, E.V., Mello, M.R., Koike, L., Marsaioli, A.J., Reis, F.A.M., 1999. 3-Alkyl and 3-carboxyalkyl steranes in marine evaporitic oils of the Potiguar Basin, Brazil. *Chemical Geology* 158, 1–20.
- Lopes, J.A.D., Santos Neto, E.V., Mello, M.R., Reis, F.A.M., 1997. Geosteranes: Identification and synthesis of a novel series of 3-substituted steranes. *Organic Geochemistry* 26, 787–790.
- Marshall, A.G., Rodgers, R.P., 2008. Petroleomics: Chemistry of the underworld. *Proceedings of the National Academy of Sciences of the United States of America* 105, 18090–18095.
- Marshall, A.G., Hendrickson, C.L., Emmett, M.R., Rodgers, R.P., Blakney, G.T., Nilsson, C.L., 2007. Fourier transform ion cyclotron resonance: state of the art. *European Journal of Mass Spectrometry* 13, 57–59.
- Marshall, A.G., Rodgers, R.P., 2004. Petroleomics: the next grand challenge for chemical analysis. *Accounts of Chemical Research* 37, 53–59.
- Martins, L.L., Pudenzi, M.A., da Cruz, G.F., Nascimento, H.D.L., Eberlin, M.N., 2017. Assessing biodegradation of Brazilian crude oils via characteristic profiles of O_1 and O_2 compound classes: petroleomics by negative-ion mode electrospray ionization Fourier Transform ion cyclotron resonance mass spectrometry. *Energy & Fuels* 31, 6649–6657.
- Martins, L.L., Schulz, H.-M., Severiano Ribeiro, H.J.P., de Souza, E.S., do Nascimento, C.A., da Cruz, G.F., 2019. Chromans as signals of freshwater incursions promoting salinity stratification in the Lower Permian Iriti Formation, Paraná Basin. *Extended Abstracts of the 29th International Meeting on Organic Geochemistry*, Gothenburg, Sweden.
- Martins, L.L., Schulz, H.-M., Severiano Ribeiro, H.J.P., do Nascimento, C.A., de Souza, E.S., da Cruz, G.F., 2020a. Organic Geochemical signals of freshwater dynamics controlling salinity stratification in organic-rich shales in the Lower Permian Iriti Formation (Paraná Basin, Brazil). *Organic Geochemistry* 140, 103958.
- Martins, L.L., Schulz, H.-M., Severiano Ribeiro, H.J.P., do Nascimento, C.A., de Souza, E.S., da Cruz, G.F., 2020b. Cadalenes and norcadalenes in organic-rich shales of the Permian Iriti Formation (Paraná Basin, Brazil): tracers for terrestrial input, or also indicators of temperature controlled organic-inorganic interactions? *Organic Geochemistry* 140, 103962.
- Martins, C.M.S., Cerqueira, J.R., Ribeiro, H.J.P.S., Garcia, K.S., da Silva, N.N., Queiroz, A.F.S., 2020c. Evaluation of thermal effects of intrusive rocks on the kerogen present in the black shales of Iriti Formation (Permian), Paraná Basin, Brazil. *Journal of South American Earth Sciences* 100, 102559.
- Matos, S.A., Warren, L.V., Varejão, F.G., Assine, M.L., Simões, M.G., 2017. Permian endemic bivalves of the “Iriti anoxic event”, Paraná Basin, Brazil: Taphonomical, paleogeographical and evolutionary implications. *Palaeogeography, Palaeoclimatology, Palaeoecology* 469, 18–33.
- Mello, M.R., Koutsoukos, E.A.M., Santos Neto, E.V., Silva Telles, A.C., 1993. Geochemical and micropaleontological characterization of lacustrine and marine hypersaline environments from Brazilian sedimentary basins. In: Katz, B.J., Pratt, L.M. (Eds.), *Source Rocks in a Sequence Stratigraphic Framework*. American Association of Petroleum Geologists, Tulsa, OK, pp. 17–34.

- Milani, E.J., França, A.B., Medeiros, R.A., 2007a. Source rocks and reservoir rocks of the Paraná Basin, eastern belt of outcrops, Paraná State. *Roteiros Geológicos (in memoriam)*. Boletim de Geociências da Petrobras 15, 135–162.
- Milani, E.J., de Melo, J.H.G., de Souza, P.A., Fernandes, L.A., Franca, A.B., 2007b. Paraná Basin. Boletim de Geociências da Petrobras 15, 265–287.
- Niyonsaba, E., Manheim, J.M., Yerabolu, R., Kenttamaa, H.I., 2019. Recent advances in petroleum analysis by mass spectrometry. *Analytical Chemistry* 91, 156–177.
- Oldenburg, T.B.P., Brown, M., Bennett, B., Larter, S.R., 2014. The impact of thermal maturity level on the composition of crude oils, assessed using ultra-high resolution mass spectrometry. *Organic Geochemistry* 75, 151–168.
- Orr, W.L., Sinnighe Damsté, J.S., 1990. Geochemistry of sulfur in petroleum systems. In Orr, W.L., White, C.M. (Eds.), *Geochemistry of Sulfur in Fossil Fuels*. ACS Symposium Series No. 429, American Chemical Society, Washington, D.C., pp. 2–29.
- Peters, K.E., Moldowan, J.M., 1991. Effects of source, thermal maturity, and biodegradation on the distribution and isomerization of homohopanes in petroleum. *Organic Geochemistry* 17, 47–61.
- Poetz, S., Horsfield, B., Wilkes, H., 2014. Maturity-driven generation and transformation of acidic compounds in the organic-rich Posidonia Shale as revealed by electrospray ionization Fourier transform ion cyclotron resonance mass spectrometry. *Energy & Fuels* 28, 4877–4888.
- Qian, K., Robbins, W.K., Hughey, C.A., Cooper, H.J., Rodgers, R.P., Marshall, A.G., 2001. Resolution and identification of elemental compositions for more than 3000 crude acids in heavy petroleum by negative-ion microelectrospray high-field Fourier Transform ion cyclotron resonance mass spectrometry. *Energy & Fuels* 15, 1505–1511.
- Radke, M., Willsch, H., Welte, D.H., 1980. Preparative hydrocarbon group type determination by automated medium pressure liquid chromatography. *Analytical Chemistry* 52, 406–411.
- Rao, Z., Qiang, M., Jia, G., Li, Y., Dan, D., Chen, F., 2016. A 15 ka lake water δD record from Genggahai Lake, northeastern Tibetan Plateau, and its paleoclimatic significance. *Organic Geochemistry* 97, 5–16.
- Reis, D.E.S., Rodrigues, R., Moldowan, J.M., Jones, C.M., Brito, M., Cavalcante, D.C., Portela, H.A., 2018. Biomarkers stratigraphy of Iratí Formation (Lower Permian) in the southern portion of Paraná Basin (Brazil). *Marine and Petroleum Geology* 95, 110–138.
- Rieley, G., Collier, R.J., Jones, D.M., Eglington, G., 1991. The biogeochemistry of Ellesmere Lake, U.K.-I: source correlation of leaf wax inputs to the sedimentary lipid record. *Organic Geochemistry* 17, 901–912.
- Rocha, Y.S., Pereira, R.C.L., Mendonça Filho, J.G., 2018. Geochemical characterization of lacustrine and marine oils from off-shore Brazilian sedimentary basins using negative-ion electrospray Fourier transform ion cyclotron resonance mass spectrometry (ESI FTICR-MS). *Organic Geochemistry* 124, 29–45.
- Rocha, Y.S., Pereira, R.C.L., Mendonça Filho, J.G., 2019. Geochemical assessment of oils from the Mero Field, Santos Basin, Brazil. *Organic Geochemistry* 130, 1–13.
- Rocha-Campos, A.C., Basei, M.A., Nutman, A.P., Kleiman, L.E., Varella, R., Llambias, E., Canile, F.M., Da Rosa, O.C.R., 2011. 30 million years of Permian volcanism recorded in the Chojoi igneous province (W Argentina) and their source for younger ash fall deposits in the Paraná Basin: SHRIMP U-Pb zircon geochronology evidence. *Gondwana Research* 19, 509–523.
- Rodgers, R.P., Schaub, T.M., Marshall, A.G., 2005. Petroleomics: MS returns to its roots. *Analytical Chemistry* 77, 22–27.
- Rodgers, R.P., McKenna, A.M., 2011. Petroleum analysis. *Analytical Chemistry* 83, 4665–4687.
- Rullkötter, J., 1993. The thermal alteration of kerogen and the formation of oil. In: Engel, M.H., Macko, S.A. (Eds.), *Organic Geochemistry: Principles and Applications*. Plenum Press, New York, pp. 377–396.
- Santos, R.V., Souza, P.A., Alvarenga, C.J.S., Dantas, E.L., Pimentel, M.M., Oliveira, C.G., Araújo, L.M., 2006. Shrimp U-Pb zircon dating and palynology of bentonitic layers from the Permian Iratí Formation, Paraná Basin, Brazil. *Gondwana Research* 9, 456–463.
- Schaeffer, P., Fache-Dany, F., Trendel, J.M., Albrecht, P., 1993. Polar constituents of organic matter rich marls from evaporitic series of the Mulhouse basin. *Organic Geochemistry* 20, 1227–1236.
- Shi, Q., Zhao, S., Xu, Z., Chung, K.H., Zhang, Y., Xu, C., 2010. Distribution of acids and neutral nitrogen compounds in a Chinese crude oil and its fractions: characterized by negative-ion electrospray ionization Fourier transform ion cyclotron resonance mass spectrometry. *Energy & Fuels* 24, 4005–4011.
- Simoneit, B.R.T., Leif, R.N., Ishiwatari, R., 1996. Phenols in hydrothermal petroleums and sediment bitumen from Guaymas Basin, Gulf of California. *Organic Geochemistry* 24, 377–388.
- Smith, D.F., Podgorski, D.C., Rodgers, R.P., Blakney, G.T., Hendrickson, C.L., 2018. 21 Tesla FT-ICR mass spectrometer for ultrahigh-resolution analysis of complex organic mixtures. *Analytical Chemistry* 90, 2041–2047.
- Sousa, J.J.F., Vugman, N.V., Neto, C.C., 1997. Free radical transformation in the Irati oil shale due to diabase intrusion. *Organic Geochemistry* 26, 183–189.
- Terra, L.A., Filgueiras, P.R., Tose, L.V., Romão, W., De Souza, D.D., De Castro, E.V.R., De Oliveira, M.S.L., Dias, J.C.M., Poppi, R.J., 2014. Petroleomics by electrospray ionization FT-ICR mass spectrometry coupled to partial least squares with variable selection methods: prediction of the total acid number of crude oils. *Analyst* 139, 4908–4916.
- Tissot, B.P., Welte, D.H., 1984. *Petroleum Formation and Occurrence*. Springer-Verlag, Berlin, Heidelberg.
- Tomczyk, N.A., Winans, R.E., Shinn, J.H., Robinson, R.C., 2001. On the nature and origin of acidic species in petroleum. 1. Detailed acid type distribution in a California crude oil. *Energy & Fuels* 15, 1498–1504.
- Tulipani, S., Grice, K., Greenwood, P.F., Schwark, L., Böttcher, M.E., Summons, R.E., Foster, C.B., 2015. Molecular proxies as indicators of freshwater incursion-driven salinity stratification. *Chemical Geology* 409, 61–68.
- Vanini, G., Barra, T.A., Souza, L.M., Madeira, N.C.L., Gomes, A.O., Romão, W., Azevedo, D.A., 2020. Characterization of nonvolatile polar compounds from Brazilian oils by electrospray ionization with FT-ICR MS and Orbitrap-MS. *Fuel* 282, 118790.
- Vaz, B.G., Abdelnur, P.V., Rocha, W.F.C., Gomes, A.O., Pereira, R.C.L., 2013a. Predictive petroleomics: Measurement of the total acid number by electrospray Fourier transform mass spectrometry and chemometric analysis. *Energy & Fuels* 27, 1873–1880.
- Vaz, B.G., Silva, R.C., Klitzke, C.F., Simas, R.C., Nascimento, H.D.L., Pereira, R.C.L., Garcia, D.F., Eberlin, M.N., Azevedo, D.A., 2013b. Assessing biodegradation in the Llanos Orientalis crude oils by electrospray ionization ultrahigh resolution and accuracy Fourier transform mass spectrometry and chemometric analysis. *Energy & Fuels* 27, 1277–1284.
- Wakeham, S.G., Sinnighe Damsté, J.S., Kohnen, M.E.L., Leeuw, J.W., 1995. Organic Sulfur compounds formed during early diagenesis in Black Sea sediments. *Geochimica et Cosmochimica Acta* 59, 521–533.
- Wan, Z., Li, S., Pang, X., Dong, Y., Wang, Z., Chen, X., Meng, X., Shi, Q., 2017. Characteristics and geochemical significance of heteroatom compounds in terrestrial oils by negative-ion electrospray Fourier transform ion cyclotron resonance mass spectrometry. *Organic Geochemistry* 111, 34–55.
- Wang, M., Zhu, G., 2019. Characterization of acidic compounds in ancient shale of Cambrian Formation using Fourier transform ion cyclotron resonance mass spectrometry, Tarim Basin, China. *Energy & Fuels* 33, 1083–1089.
- Weiss, H.M., Wilhelms, A., Mills, N., Scotchmer, J., Hall, P.B., Lind, K., Brekke, T., 2000. NIGOGA—The Norwegian Industry Guide to Organic Geochemical Analysis. Edition 4.0. Norsk Hydro, Statoil, Geolab Nor, SINTEF Petroleum Research and the Norwegian Petroleum Directorate.
- Zalán, P.V., Wolff, S., Astolfi, M.A.M., Vieira, I.S., Conceição, J.C.J., Appi, V.T., Santos Neto, E.V., Cerqueira, J.R., Marques, A., 1990. The Paraná Basin, Brazil. In: Leighton, M.W., Kolata, D.R., Oltz, D.F., Eidel, J.J. (Eds.), *Interior Cratonic Basins*. AAPG Memoir 51, 681–708.
- Zhang, Y., Wang, Y., Ma, W., Lu, J., Liao, Y., Li, Z., Shi, Q., 2019. Compositional characterization of expelled and residual oils in the source rocks from oil generation-expulsion thermal simulation experiments. *ACS Omega* 4, 8239–8248.
- Zhang, Y., Liao, Y., Guo, S., Xu, C., Shi, Q., 2016. Molecular transformation of crude oil in confined pyrolysis system and its impact on migration and maturity geochemical parameters. *Energy & Fuels* 30, 6923–6932.
- Zhang, Y., Shi, Q., Li, A., Chung, K.H., Zhao, S., Xu, C., 2011. Partitioning of crude oil acidic compounds into subfractions by extrography and identification of isoprenoid phenols and tocopherols. *Energy & Fuels* 25, 5083–5089.
- Zhang, C., Zhang, Y., Zhang, M., Zhao, H., Cai, C., 2008. Carbazole distributions in rocks from non-marine depositional environments. *Organic Geochemistry* 39, 868–878.
- Ziegs, V., Noah, M., Poetz, S., Horsfield, B., Hartwig, A., Rinna, J., Skeie, J.E., 2018a. Unravelling maturity- and migration-related carbazoles and phenol distributions in Central Graben crude oils. *Marine and Petroleum Geology* 94, 114–130.
- Ziegs, V., Poetz, S., Horsfield, B., Rinna, J., Hartwig, A., Skeie, J.E., 2018b. Deeper insights into oxygen-containing compounds of the Mandal Formation, Central Graben, Norway. *Energy & Fuels* 32, 12030–12048.